nature microbiology

Article

https://doi.org/10.1038/s41564-025-01966-0

Pseudomonas syringae subpopulations cooperate by coordinating flagellar and type III secretion spatiotemporal dynamics to facilitate plant infection

Received: 19 March 2024

Accepted: 19 February 2025

Published online: 2 April 2025

Check for updates

Nieves López-Pagán[1,7], José S. Rufián[1], Julien Luneau[2,3], María-Antonia Sánchez-Romero[4], Laurent Aussel[5], Simon van Vliet[2,6], Javier Ruiz-Albert[1] & Carmen R. Beuzón[1]

Isogenic bacterial populations can display probabilistic cell-to-cell variation in response to challenges. This phenotypic heterogeneity can affect virulence in animals, but its impact on plant pathogens is unknown. Previously, we showed that expression of the type III secretion system (T3SS) of the plant pathogen *Pseudomonas syringae* displays phenotypic variation in planta. Here we use flow cytometry and microscopy to investigate single-cell flagellar expression in relation to T3SS expression, showing that both systems undergo phenotypic heterogeneity in vitro in apoplast-mimicking medium and within apoplastic microcolonies throughout colonization of *Phaseolus vulgaris*. Stochastic, spatial and time factors shape the dynamics of a phenotypically diverse pathogen population that displays division of labour during colonization: effectors produced by T3SS-expressing bacteria act as 'common goods' to suppress immunity, allowing motile flagella-expressing bacteria to increase and leave infected tissue before necrosis. These results showcase the mechanisms of bacterial specialization during plant colonization in an environmentally and agriculturally relevant system.

Flagellar motility is an important trait for environmental adaptation. Members of the genus *Pseudomonas* can colonize soil, plant or animal tissues. The *Pseudomonas syringae* species complex includes most of those pathogenic to plants, collectively causing diseases in over 500 species, many agriculturally relevant[1]. *P. syringae* can live on the leaf surface, but most favour endophytic colonization, using wounds and stomata to enter the leaf. Flagellar motility confers advantages to epiphytic populations of *P. syringae* pv. *syringae*[2] and facilitates leaf entry for many *P. syringae* pathovars[3,4]. Inside the leaf, *P. syringae* colonizes the intercellular spaces (apoplast). Once inside, flagellar motility is not required for systemic spread[3], while flagellin, the main component of the pilus, triggers immunity[5]. Fittingly, flagellar expression is down-regulated in the apoplast[6–8].

Flagellar biosynthesis is depicted as a deterministic programme with a complex and tiered regulatory hierarchy, where promoters are sequentially activated, maintaining this state through active growth.

[1]Instituto de Hortofruticultura Subtropical y Mediterránea "La Mayora", Universidad de Málaga-Consejo Superior de Investigaciones Científicas (IHSM-UMA-CSIC), Málaga, Spain. [2]Department of Computational Biology, University of Lausanne, Lausanne, Switzerland. [3]Department of Fundamental Microbiology, University of Lausanne, Lausanne, Switzerland. [4]Departamento de Microbiología y Parasitología, Facultad de Farmacia, Universidad de Sevilla, Sevilla, Spain. [5]Aix Marseille Univ, CNRS, LCB UMR7283, IMM, Marseille, France. [6]Biozentrum, University of Basel, Basel, Switzerland. [7]Present address: Department of Chemical Biology and Genetics, Centre of the Region Haná for Biotechnological and Agricultural Research, Faculty of Science, Palacký University, Olomouc, Czech Republic. e-mail: cbeuzon@uma.es

However, single-cell studies revealed stochastic activation pulses and bimodal patterns in the flagellar system of *Salmonella enterica*, with clonal populations displaying phenotypic heterogeneity[9–13]. In *P. syringae*, regulation of flagellar synthesis remains mostly uncharacterized, but gene arrangement and promoter conservation with *P. putida* supports a similar hierarchy of transcriptional regulation[14], with FleQ at the top[15].

Apoplastic *P. syringae* use a type III secretion system (T3SS) to introduce effectors (T3Es) into the host-cell cytosol. T3Es suppress plant immunity including flagellin-triggered responses, allowing bacterial proliferation and disease[16]. T3SS gene expression requires HrpL[17]. We showed that a *ΔhrpL* mutant displays increased swimming motility in apoplast-mimicking Hrp-inducing medium (HIM), while a mutant lacking HrpV, a repressor of *hrpL* expression[18], displays reduced motility[19], suggesting a regulatory link between T3SS and flagellar expression. Later, we established that *P. syringae* T3SS genes display phenotypic heterogeneity during plant colonization and bistable expression with reversible ON and OFF states in HIM[20].

Here we show that flagellar gene expression displays phenotypic heterogeneity in *P. syringae*, particularly within the plant apoplast. While average expression levels of flagellin-encoding *fliC* is downregulated in the apoplastic population, as previously described[6–8], a subpopulation expresses high *fliC* levels during colonization. Analysing flagellar and T3SS expression simultaneously, we found all possible single-cell ON/OFF combinations, revealing the phenotypic complexity arising amid clonal populations. Nonetheless, T3SS^{ON}/Flagella^{OFF} and T3SS^{OFF}/Flagella^{ON} subpopulations were generally more abundant, suggesting counter-regulation between these loci. Expression of these systems impacts bacterial growth at the population and/or cellular level. Analysis of the spatial distribution of expression within apoplastic microcolonies shows that T3SS^{ON} bacteria are more abundant early in the infection and close to the host-cell surface, while Flagella^{ON} bacteria become more frequent later and further away from the host cell. Following bacterial apoplastic multiplication, Flagella^{ON} bacteria actively exit the infected tissue before the onset of necrotic symptoms. Our results support a division of labour model with T3SS^{ON} secreted effectors acting as common goods, allowing Flagella^{ON} bacteria to increase and exit before tissue collapse.

Results

Flagellar expression in *P. syringae* is heterogeneous

We generated a transcriptional fusion to *GFP3* (AAB18957.1) of flagellin-encoding *fliC* (WP_002554301.1) within its genome location, preserving context and function without affecting fitness or virulence (Extended Data Fig. 1) in model bean pathogen *P. syringae* pv. *phaseolicola* 1448A[21]. Using confocal laser scanning microscopy (CLSM) and flow cytometry (FC), we monitored *fliC::GFP3* expression in vitro (Fig. 1a). In rich lysogeny broth (LB) medium and apoplast-mimicking HIM medium, most bacteria express *fliC::GFP3* (Flagella^{ON}) with considerable cell-to-cell variation, but a subpopulation does not (Flagella^{OFF}) and can be visualized only by membrane staining, overlapping with non-fluorescent bacteria in FC analyses (Fig. 1a). Expression of *GFP3* from a constitutive promoter is homogeneous[22], ruling out expression noise as the *fliC::GFP3* source of heterogeneity.

In keeping with flagellar role in facilitating leaf entry[2–4], leaf-surface bacteria are mostly Flagella^{ON}. Nonetheless, images of bean (*Phaseolus vulgaris*) leafs sprayed with *fliC::GFP3* bacteria constitutively expressing eCFP show that flagellar expression is also heterogeneous on leaf surfaces (Extended Data Fig. 2). Four days post pressure inoculation (dpi), bacteria recovered from the apoplast display lower average expression than media-grown populations (Fig. 1b), agreeing with transcriptomic data[6–8]. However, most apoplast-extracted bacteria are Flagella^{ON} (Fig. 1a). Cell-to-cell differences in fluorescence were more pronounced among apoplast-extracted bacteria than in media, with a wider distribution revealed by FC (Fig. 1a (right),c). This variability is also apparent in planta, with apoplastic microcolonies of *fliC::GFP3* eCFP bacteria showing heterogeneous GFP3 fluorescence overlaid with homogeneous eCFP fluorescence distribution (Fig. 1d). Homogeneous *eCFP* expression was reported previously[23].

LB populations were sorted by fluorescence-activated cell sorting based on GFP fluorescence (Fig. 1e), enriching populations with low or high *fliC::GFP3* expression (Fig. 1e right) to use in swimming assays. Since sorting causes physical flagellar damage, it can reduce motility differences between sorted subpopulation pairs and increase variation between sorting events. Thus, we compared motility between high/low subpopulations separated in the same sorting event (Fig. 1f): we calculated the ratio between swimming halo diameters of high GFP3- and low GFP3-expressing subpopulations (per sorted event). High-to-low motility ratios for sorted LB populations were significantly higher than 1.0, indicating that *fliC* expression positively correlates with motility (Fig. 1f). Similar results were obtained using HIM populations (Fig. 1g,h). These results indicate that flagella are phenotypically heterogeneous in *P. syringae* and show that, despite flagellin being an immune elicitor, part of the apoplastic population expresses flagella.

Flagella and T3SS show counter-regulation at the cellular level

Next, we used a strain carrying transcriptional fusions *fliC::tdT* (to *tdTomato*; AAV52169 1) and *hrpL::GFP3* (WP_004656240.1) to evaluate T3SS and flagella expression simultaneously. Population profiles for *fliC::tdT* are similar to those of *fliC::GFP3* (Extended Data Fig. 3a,b). Potential interferences between fluorophores (that is, bleedthrough leading to false positives or Förster resonance energy transfer (FRET) leading to false negatives) were ruled out (Extended Data Fig. 3c,d). Both systems were expressed heterogeneously in HIM (Fig. 2a,b (left) and Extended Data Fig. 3e). FC showed two subpopulations, formed by bacteria favouring expression of T3SS (T3SS^{ON}/Flagella^{OFF}) or *fliC*

Fig. 1 | Flagella display phenotypic heterogeneity in *Pseudomonas syringae*. **a**, Left: CLSM images and FC analysis of bacteria carrying *fliC::GFP3* grown in LB or HIM medium, or apoplast extracted from leaf apoplasts at 4 dpi. FM4-64 channel (greyscale) display fluorescence from membrane staining. Scale bars, 2 µm. Right: FC data obtained from *fliC::GFP3* bacteria are represented using arbitrary units in logarithmic scale. Non-GFP graphs show autofluorescence levels of wild type as reference for OFF subpopulations (vertical lines leave 99% non-GFP data to the left). Microscopy and FC panels show typical results ($n = 14$ independent experiments). **b**, Mean GFP fluorescence intensity of *fliC::GFP3*-carrying bacterial populations ($n = 14$) from FC data described in **a**. **c**, Robust coefficient of variation (RCV) obtained from FC data described in **a**. **b** and **c** display individual sample values, and sample sets displaying different letters are significantly different as determined using one-way analysis of variance (ANOVA) followed by Tukey's multiple comparisons test ($P < 0.05$); all comparisons showed $P < 0.0001$. Lines indicate the means of all individual data. Error bars represent s.e.m. **d**, CLSM images of *fliC::GFP3* bacteria expressing a constitutive *eCFP* gene growing in microcolonies in planta at 3 dpi. GFP channel shows heterogeneous distribution of *fliC* expression. CFP channel shows homogeneous distribution of CFP ($n = 3$). Red in all panels corresponds to chloroplast autofluorescence. Scale bars, 5 µm. In **a** and **d**, contrast and brightness were adjusted to improve visualization and kept constant across samples and channels. **e**,**g**, Histograms showing GFP fluorescence vs cell count from *fliC::GFP3* overnight LB-grown cultures (**e**) or 24 h HIM-grown cultures (**g**) before (left) and after (right) sorting. Red lines indicate gating used to separate *fliC::GFP3* bacteria according to fluorescence intensity. **f**,**h**, Relative ratio between halo diameters in swimming plates seeded with cells displaying high GFP expression, divided by the diameters of halos obtained from seeding cells displaying low GFP expression, resulting from the same sorting event (identified with different shades) from cultures grown in LB (**f**) or HIM (**h**) ($n = 9$ as shown). Lines indicate the means of all individual data. Error bars represent s.e.m. Asterisks indicate significant differences established by an unpaired two-tailed *t*-test ($P < 0.05$). *P* values are indicated.

https://doi.org/10.1038/s41564-025-01966-0

(T3SS^{OFF}/Flagella^{ON}) (Fig. 2a,b (left)). Although these combinations were more abundant, a continuous distribution with bacteria expressing both (T3SS^{ON}/Flagella^{ON}) or none (T3SS^{OFF}/Flagella^{OFF}) was observed (Fig. 2a,b (left) and Extended Data Fig. 3e). Apoplast-extracted bacteria (4 dpi) also displayed all phenotypic combinations, although T3SS^{ON}/Flagella^{OFF} bacteria were more abundant (Fig. 2a,b (right)). As reported[20], apoplastic populations did not display bimodal GFP distribution (Fig. 2a,b and Extended Data Fig. 3f). Analysis of T3SS effector gene *hopAB1* (ref. 20)(WP_011282445.1) rendered similar results (Fig. 2c,d and Extended Data Fig. 3e,f).

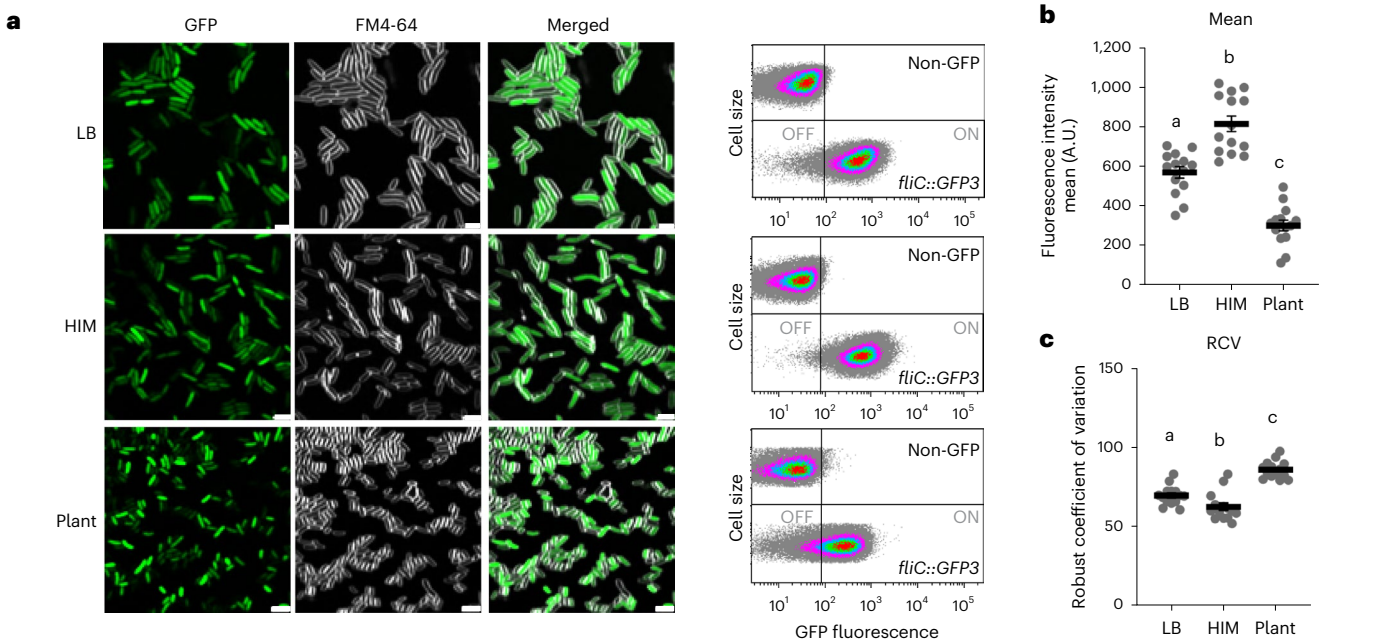

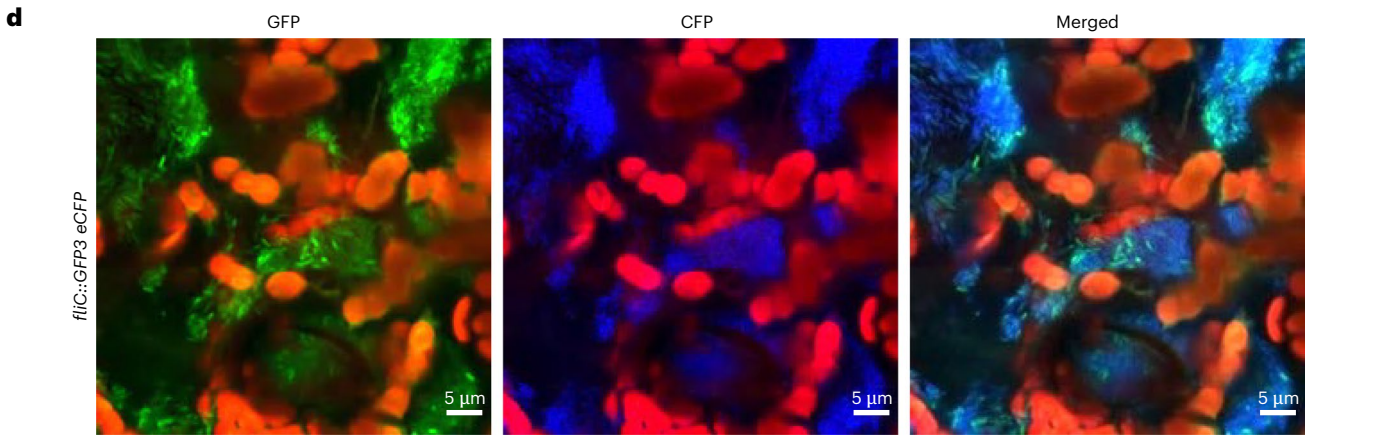

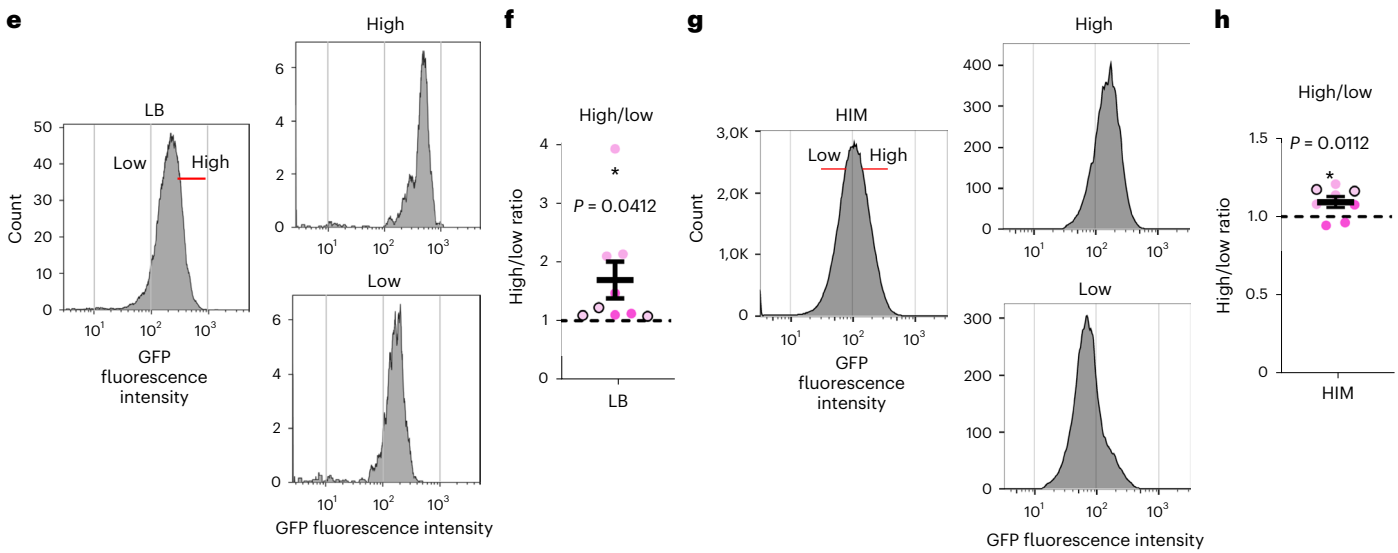

https://doi.org/10.1038/s41564-025-01966-0

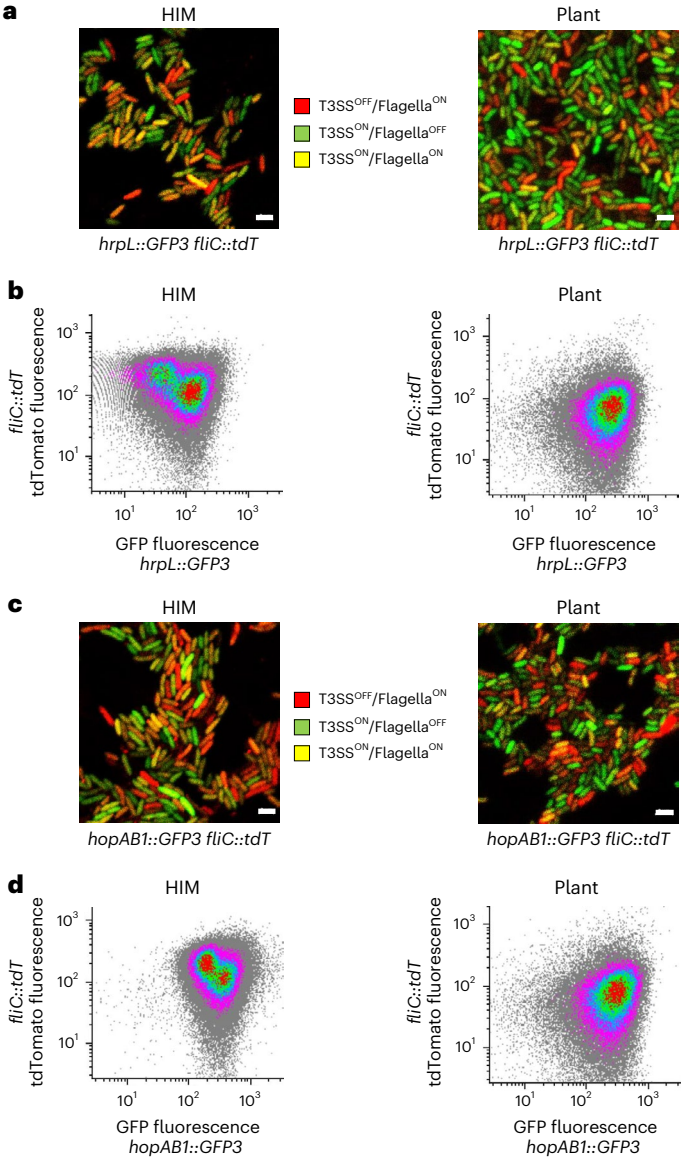

Fig. 2 | Flagellar and T3SS expression display independent heterogeneous expression at the single-cell level. a, CLSM images of dual-reporter *hrpL::GFP3 fliC::tdT* strain grown in HIM or extracted from leaf apoplasts at 4 dpi. Scale bars, 2 µm. Contrast and brightness were adjusted to improve visualization and used throughout. **b**, FC analysis of bacteria described in **a**. Graphs show GFP fluorescence intensity vs that of tdTomato. Results shown in the figure are representative of 3 or more independent experiments. **c**, CLSM images of dual-reporter *hopAB1::GFP3 fliC::tdT* strain grown in HIM or extracted from leaf apoplasts at 4 dpi. Scale bars, 2 µm. Contrast and brightness were adjusted to improve visualization and used throughout. **d**, FC analysis of bacteria described in **c**. Results shown in the figure are representative of at least 3 independent experiments.

Expression of T3SS or flagella carries growth penalties

Expression of *Salmonella* pathogenicity island 1 (SPI1) T3SS causes growth delays, which have been proposed to drive phenotypic heterogeneity[24,25]. We used competitive index (CI) assays (Fig. 3a) to compare growth of a *ΔhrpL* mutant and wild-type bacteria (Fig. 3b). CIs show that *ΔhrpL* mutants outgrow wild-type bacteria in HIM (CI = 1.75 ± 0.15), but not in rich medium (CI = 1.07 ± 0.08), where T3SS genes are not expressed. Growth rates of *ΔhrpL* bacteria are also higher in HIM (Fig. 3c). In planta, wild-type bacteria outgrow a derivative constitutively expressing HrpL (CI = 0.67 ± 0.06) (Fig. 3d). Constitutive expression of HrpL results in overexpression of T3SS genes[20], supporting that T3SS expression carries a growth penalty.

Flagella often carries growth penalties[26–28]. However, previous CI assays did not show significant growth differences for *ΔfliC* bacteria in *P. syringae*[29]. Fittingly, we did not observe significant growth differences for *ΔfliC* or *ΔfleQ* (WP_011169094.1) (lacking flagellar regulator FleQ) mutants based on CI (LB: CI = 1.08 ± 0.22 and 1.00 ± 0.13, respectively; HIM: CI = 1.21 ± 0.22 and 1.31 ± 0.13, respectively), although variation in LB *ΔfliC* CI was large (Fig. 3b), or growth rates (Extended Data Fig. 4a). However, a *ΔhrpL ΔfliC* mutant remarkably outgrows wild type, with CI values (LB: CI = 4.195 ± 0.9975: HIM: CI = 25.79 ± 5.156) 4–15 fold those obtained for single *ΔhrpL* mutant (Fig. 3b). This supports the notion that flagellar expression carries a cost, at least when simultaneously expressed with the T3SS. Constitutive expression of *fleQ* from pFleQ led to severe growth delays (Extended Data Fig. 4a), although pleiotropic effects could not be ruled out given the severity of the phenotype.

In plants treated with flagellin to void differences associated with flagellin-mediated immunity, CI assays revealed growth advantages for *ΔfliC* mutants (CI = 1.88 ± 0.34) (Fig. 3d). However, we cannot rule out that *ΔfliC* mutant advantages in flagellin-treated plants may stem from other reasons.

Since T3SS and flagellar expression are both highly heterogeneous, population-level assays could be noisy and may lead to underestimating growth penalties. Thus, we analysed these impacts at the single-cell level using HIM-agar pads and time-lapse microscopy. In this setting, *hopAB1::GFP3* activation takes place too late in the experiment to allow for confident quantification (Supplementary Videos 1–4). However, activation of *fliC::GFP3* takes place earlier (Supplementary Videos 5 and 6, and Fig. 3e). Time-lapse analyses show that *fliC* expression negatively correlates with bacterial growth (Fig. 3f). Splitting the *fliC::GFP3* population into two using the median fluorescence intensity value, we detected a 6.5% growth penalty for the higher-than-median-fluorescence half compared with the lower half (Fig. 3g). Constitutive expression of eGFP does not negatively correlate with growth (Extended Data Fig. 4b–f).

Phenotypic specialization during microcolony development

Apoplastic Flagella^{ON}/T3SS^{OFF} subpopulations are potentially more vulnerable to plant defences since they trigger but cannot suppress immunity. We used propidium iodide which binds to membrane-compromised (not viable) bacteria to determine any correlation between phenotypic variants and apoplast killing rates[30,31]. No significant differences were observed between dead/live ratios of Flagella or T3SS ON vs OFF subpopulations (Extended Data Fig. 5), supporting that Flagella^{ON}/T3SS^{OFF} cells are protected from plant responses, perhaps by T3SS^{ON} bacteria suppressing defences in *trans*.

We established that T3SS mutant bacteria may proliferate up to wild-type levels when growing within the same microcolony as wild-type bacteria[22], while wild-type and T3SS mutant bacteria growing in separate microcolonies develop according to their respective abilities to suppress local immunity. Therefore, *trans* complementation between T3SS^{ON} and Flagella^{ON}/T3SS^{OFF} bacteria would require phenotypic variants to rise during growth of the microcolony. Fluorescence distribution of *fliC:GFP3* in planta shows that for flagella, ON/OFF variants appear closely located within the microcolony (Fig. 1d). Close examination of *fliC::GFP3* distribution (Supplementary Video 7) reveals areas with stronger fluorescence, suggesting a response to local stimuli (or siblings' inheritance of an expression pattern), but also isolated bacteria displaying GFP fluorescence strikingly different from those of nearby peers, in keeping with stochastic differences.

We followed expression of T3SS and flagella genes during the development of apoplastic microcolonies, analysing leaves infiltrated with *hopAB1::GFP3 fliC::tdT* or *hrpL::GFP3 fliC::tdT* bacteria at different timepoints (Fig. 4a,b). Stochastic T3SS heterogeneity was detected

https://doi.org/10.1038/s41564-025-01966-0

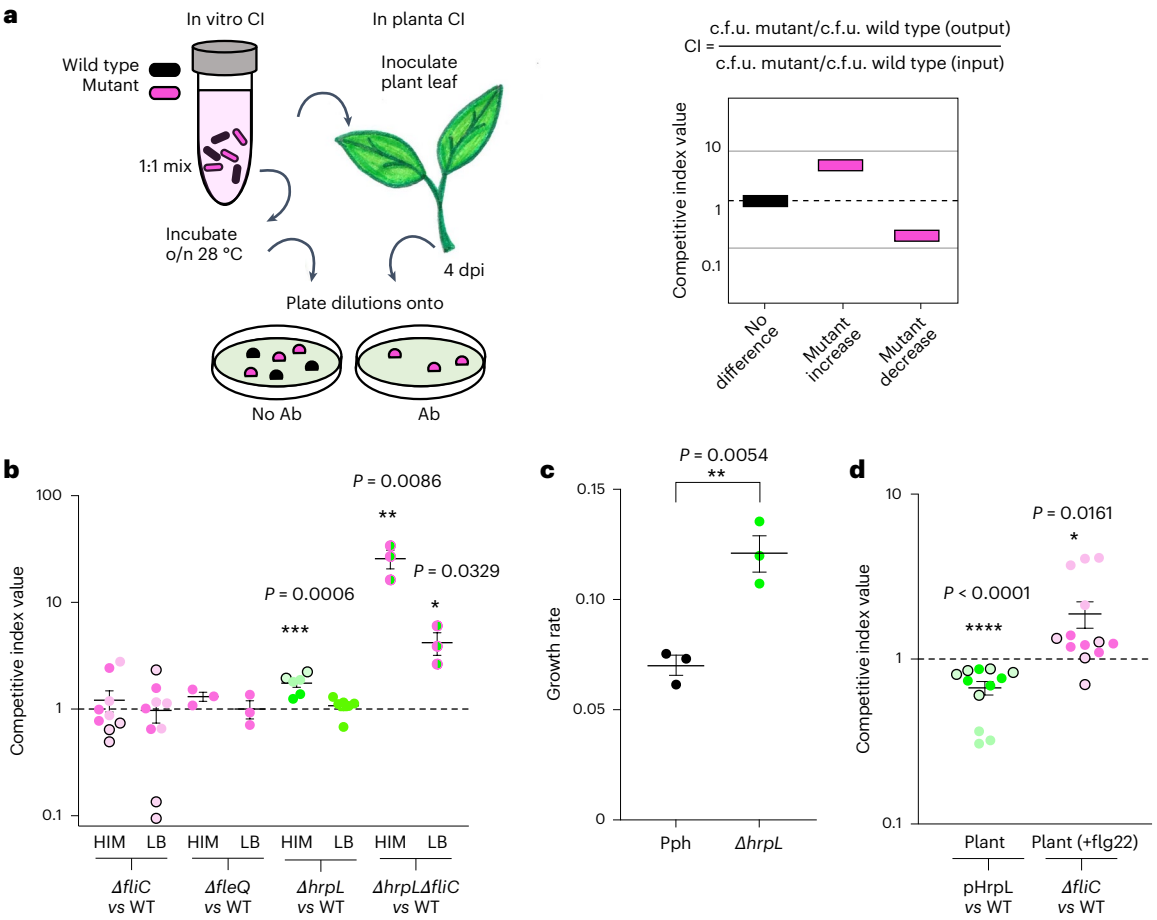

Fig. 3 | Flagellar and T3SS expression impact on bacterial growth. a, Left: competitive index assay overview: inocula containing 1:1 mixes of wild-type and mutant (or plasmid-carrying) LB-grown cultures are used to inoculate leaves (in planta CI) or to start fresh cultures (in vitro CI). Resulting mixed cultures and apoplast-extracted bacteria (4 dpi) are serially diluted and plated with or without antibiotics for c.f.u. determination (output). Right: CI is calculated as mutant-to-wild-type c.f.u. ratio in output divided by ratio in input. CIs different from 1.0 indicate strains growing significantly differently: mutant outgrowing wild type (CI > 1.0) or vice versa (<1). **b**, CIs for mutants vs wild-type strain (WT) in HIM or LB (n = 3–9 as shown). **c**, HIM growth rates for *ΔhrpL* mutant and wild type. **d**, In planta CIs for wild type constitutively expressing *hrpL* (pHrpL) or *ΔfliC*, vs WT at 4 dpi (n = 10 as shown). Plants for *ΔfliC* CI pretreated with flg22. In **b**–**d**, data show mean ± s.e.m. Individual data for each biological replicate shown; different shades identify independent experiments, and results with asterisks are significantly different from 1.0 (non-parametric two-sided Student's t-test). Significant P values indicated. **e**, Time-lapse images of *fliC::GFP3* bacteria growing on agar pads: phase-contrast channel (top), GFP fluorescence (bottom). Contrast and brightness adjusted to improve visualization and kept constant across frames. **f**, Correlation between growth rates and fluorescence intensity of individual *fliC::GFP3* cells. Each point represents a single cell, with *fliC* expression and growth rate averaged over cell lifetime. Grey-shaded area shows 95% confidence interval around linear regression model fit. Correlation tested with Pearson's correlation coefficient using two-sided test ($R = -0.17$; $P = 1.03 \times 10^{-9}$). **g**, Growth rates for high-GFP- and low-GFP-signal cells (determined by splitting the population using median fluorescence intensity) show significantly slower growth in high-GFP cells (two-sided Mann–Whitney U-test, $P = 3.6 \times 10^{-8}$). Data presented as boxplots with first and third quartiles as bottom and top bounds, median shown as horizontal line in the box, and 1.5 interquartile range shown as whiskers. Outliers not shown. Grey violin plot shows distribution of all data points summarized in boxplot. White diamonds show mean growth rate for all cells considered.

throughout, while zonal distribution of flagellar and T3SS fluorescence within the microcolonies changed over time. One-dpi microcolonies displayed heterogeneous expression of T3SS, but no flagellar expression, supporting the idea that flagella is turned off in early infection stages[6–8]. Two-dpi microcolonies displayed orange and yellow tones consistent with expression of both systems. By 3–4 dpi, predominantly red (*fliC::tdT*) or green (*hopAB1::GFP3* or *hrpL::GFP3*) zones with thoroughly overlaid heterogeneity becomes the norm (Fig. 4a,b). Zones with higher expression of *hopAB1::GFP3* generally display lower expression of *fliC::tdT* and vice versa, although there are also orange and yellow spots indicative of T3SS^{ON}/Flagella^{ON} bacteria (Fig. 4a,b). Most remarkably, this zonal distribution shows a consistent spatial pattern: bacteria closest to the lower epidermis (Fig. 4c–e), or to a spongy mesophyll host cell (Fig. 4a (right),f,g), are predominantly green, that is, T3SS^{ON}, whereas those further away from the host-cell surface, that is, the innermost or furthermost parts of the microcolonies, are predominantly red, that is, Flagella^{ON} (Fig. 4, and Supplementary Videos 8 and 9). Although the T3SS^{ON} zone in the proximal side varies in width, it is consistently wider than a single bacterial layer, supporting the idea that the signal(s) activating T3SS expression include diffusible molecules.

Flagella^{ON} bacteria actively exit infected tissues

The increase of Flagella^{ON} bacteria in older microcolonies suggests a function at later infection stages. We took leaves at 1 dpi, 2 dpi (asymptomatic), 5 dpi (onset of macroscopic symptoms) and 7 dpi (fully symptomatic) and submerged them into a sterile $MgCl_2$ solution for 30 min. We used CLSM to evaluate *hopAB1::GFP3* and *fliC::tdT* expression in those bacteria found in the solution. Bacteria exited even intact 1 dpi leaves. Shorter incubations also allowed bacterial recovery but not enough for reliable quantification. We compared T3SS or *fliC* expression between bacterial populations exiting the leaf and whole-leaf populations obtained by mechanical extraction from replicate leaves without incubation (Fig. 5 and Extended Data Fig. 6). Exiting and total apoplast-extracted populations showed similar *hopAB1::GFP3* expression profiles at 1 dpi, 2 or 7 dpi (Fig. 5a,b and Extended Data Fig. 6), while significantly fewer T3SS^{ON} bacteria were detected in the exiting fraction by 5 dpi (Extended Data Fig. 6). In contrast, bacteria exiting 1 dpi leaves were significantly enriched in Flagella^{ON} (Fig. 5a,b), even though total apoplast-extracted bacterial populations showed almost no Flagella^{ON} bacteria (Figs. 4 and 5a, and Extended Data Fig. 6). This supports the notion of Flagella^{ON} bacteria being more efficient in actively exiting the leaf in humid conditions. We confirmed this notion using an experimental setting mimicking rain or heavy dew, by spraying the infected leaves every 5 min for 30 min and collecting the dripping solution for microscopic examination (Fig. 5a bottom panels). The bias towards Flagella^{ON} bacteria in the exiting populations detected at 2 and 5 dpi and progressively decreasing until they are no longer detected at 7 dpi (Fig. 5a,b and Extended Data Fig. 6), when leaf integrity has been lost, suggests that flagellar motility is not only important for bacterial entry into the leaf but also for fast and active exit of apoplast-grown bacteria before necrosis.

Discussion

Bacterial encounters with environmental changes lead to gene activation often assumed to happen in a non-fluctuating homogeneous manner. However, studies averaging population data lose cell-to-cell variation, and an increasing number of traits have been shown to manifest differently across clonal populations. Such phenotypic variation may reflect microenvironmental differences but may also be caused

Fig. 4 | Stochastic and spatially structured time-course distribution of flagellar and T3SS expression within apoplastic microcolonies. a, CLSM Z-stack compilation at different dpi showing apoplastic microcolonies of *hopAB1::GFP3 fliC::tdT* bacteria. All images examined (n = 5 or more) per biological replicate (n = 2) and independent experiment (n = 2 for 1 and 2 dpi; n = 4 for 3 and 4 dpi). **b**, Images from **a** including orthogonal projections. The colored lines within the central images indicate the planes that generate each orthogonal section: green lines indicate the section that is displayed in the green-boxed images (images above per time point), red lines indicate the section that is displayed in the red-boxed images (images on the right per time point). In green- or red-boxed images, the blue line correspondes to the section displayed in the central image. Scale bars, 5 µm. **c**, Schematic leaf 3D structure with close-up showing location of apoplastic microcolonies. Position and orientation of Z-stack acquisition are indicated; 1–3 represent three planes of a bacterial microcolony growing from the lower epidermis inner surface inwards (1 closest to cell surface and 3 furthest) as shown in **d** and Supplementary Video 8. Plane 4 cuts through a bacterial microcolony growing wrapped around a spongy mesophyll cell (SMC) (as microcolony and frame shown in **f** and Z-stack shown in Supplementary Video 9). **d**, Frames of a Z-stack acquisition taken from an apoplastic microcolony of *hrpL::GFP3 fliC::tdT* bacteria at 4 dpi. Contrast and brightness were adjusted to improve visualization and kept constant throughout. Scale bars, 10 µm. Lower epidermis and mesophyll indicate relative position of frames within the leaf. **e**, Schematic distribution of fluorescence for *fliC::tdT* and *T3SS::GFP3* within the type of apoplastic microcolonies indicated in **c** (1–3) and shown in **d**: planes closest to lower epidermis (abaxial side) show predominantly green bacteria and those furthest predominantly red, with intermediate plane displaying yellow. Heterogeneity is observed within each plane. **f**, Z-stack frame taken from an apoplastic microcolony of *hopAB1::GFP3 fliC::tdT* bacteria (Z-stack in Supplementary Video 9) from experiments described in **a**. Scale bars, 20 µm. **g**, Schematic fluorescence distribution for *fliC::tdT T3SS::GFP3* bacteria within apoplastic microcolonies of the type indicated in **c** (4) and shown in **f**: bacteria closest to the cell are predominantly green, turning to yellow and red as they get further away. Heterogeneity is displayed throughout. In **e** and **g**, legend indicates green as T3SS^{ON}/ Flagella^{OFF} bacteria, red as T3SS^{OFF}/ Flagella^{ON} and yellow/orange as bacteria expressing both to different levels.

by stochastic cellular changes (gene expression noise) and particular regulatory circuits (enhancing noise)[32].

P. syringae produce polar flagella[33,34] upon activation of FleQ[15] under a regulatory cascade that is mostly uncharacterized. Gene arrangement and promoter motifs conservation with *P. putida*[14], which also produces polar flagella, support a similar organization. Nonetheless, we show that *P. syringae* flagellar regulation shares an important feature with that of peritrichous *Salmonella*: stochastic cell-to-cell variation (Fig. 1 and Extended Data Figs. 1–3)[9–13,35,36]. Bistable activation of *Salmonella* flagella is established by two mechanisms[9–13]: (1) a double-negative feedback loop and (2) a developmental checkpoint. A dual mechanism is also involved in turning *P. syringae*

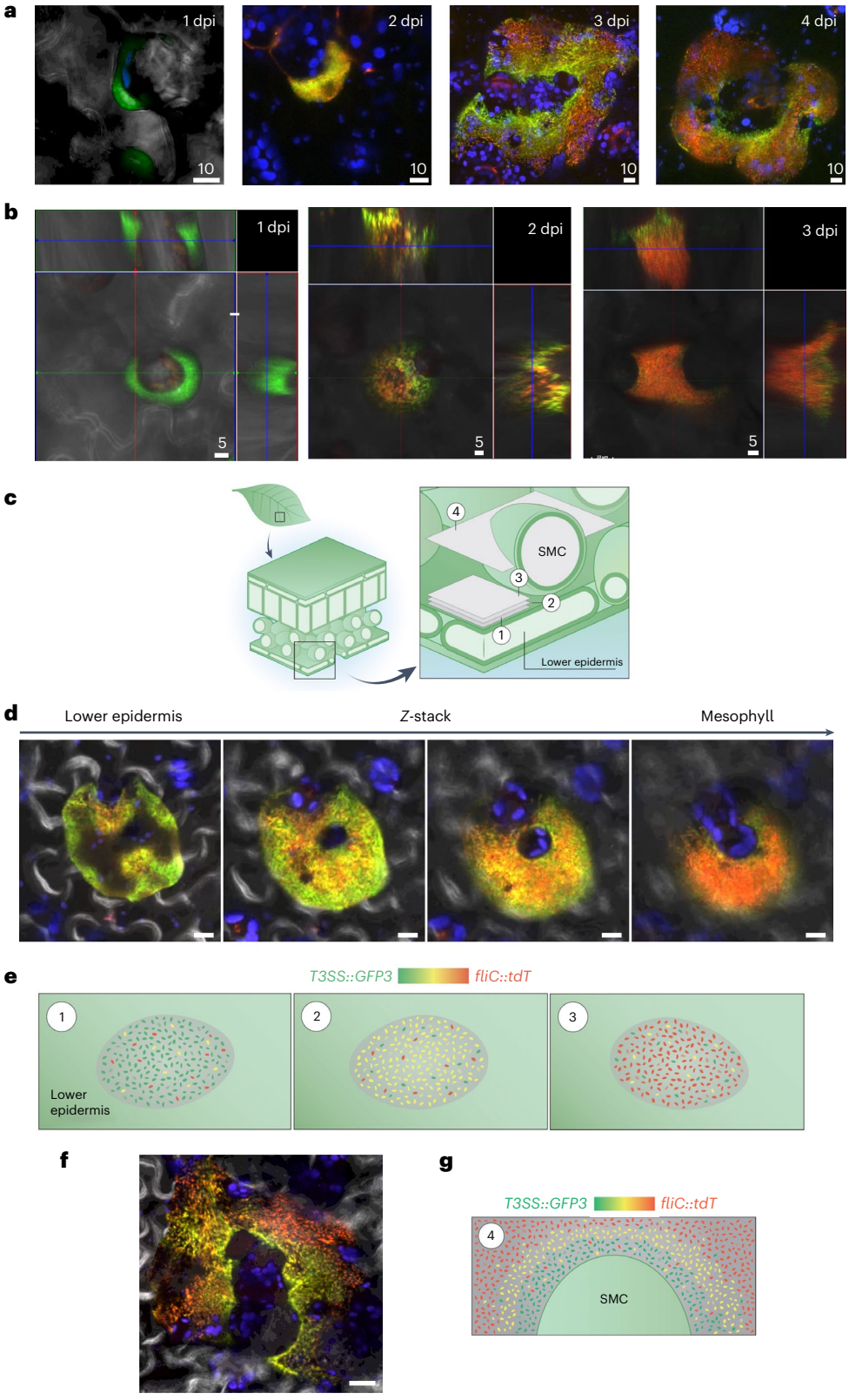

https://doi.org/10.1038/s41564-025-01966-0

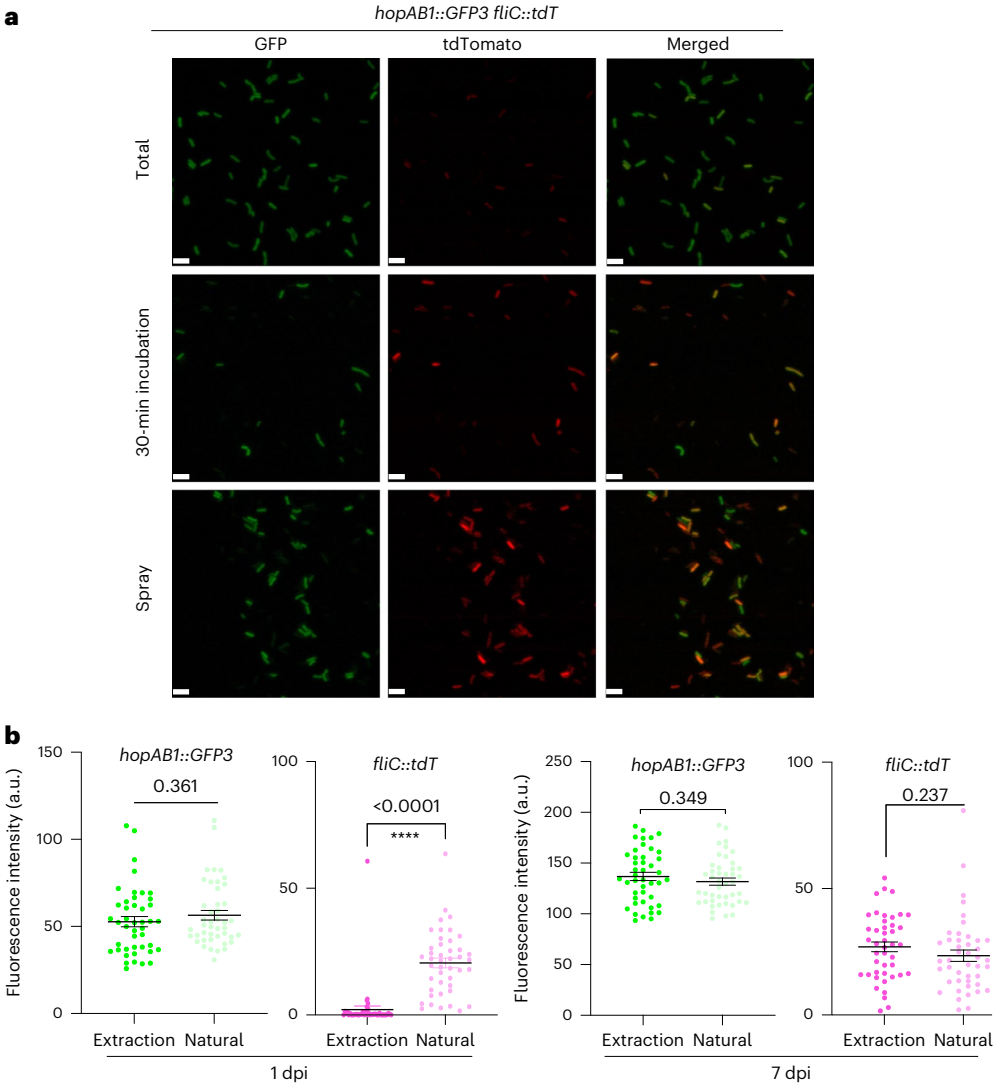

Fig. 5 | Active exit from infected tissues is carried out by Flagella^{ON} bacteria. **a**, Selected images of apoplast-extracted bacteria (using negative pressure; top panels), bacteria exiting the tissue on their own (during 30 min leaf incubation within an $MgCl_2$ solution; middle panels) or bacteria recovered from excess solution dripping from leaves sprayed every 5 min to mimic rain (bottom panels). Contrast and brightness were adjusted to improve visualization but were kept constant across the different conditions. **b**, Fluorescence quantification of the images obtained in **a** (left images) at 1 dpi (left graphs) and at 7 dpi (right graphs) of the same time-course experiment, using Fiji software. Graph shows arbitrary units of GFP fluorescence corresponding to the expression of the T3SS gene fusion *hopAB1::GFP3*, or tdTomato fluorescence corresponding to the expression of *fliC::tdT*. Each dot corresponds to an individual bacterium as analysed from the image ($n = 44$). Data are presented as mean ± s.e.m. Graphs show results representative of 5 independent experiments ($n = 2$ for strain carrying *hrpL::GFP3 fliC::tdT* and $n = 3$ for strain carrying *hopAB1::GFP3 fliC::tdT*). Comparisons between apoplast extraction and natural exit were carried out per sample using an unpaired *t*-test (****$P < 0.0001$) and results shown for each pair.

T3SS noisy expression into bimodality[20]: (1) a double-negative[18,37] and (2) a positive feedback loop[38]. Research into the regulation of flagellar synthesis in *P. syringae* will help identify elements involved in phenotypic heterogeneity.

Flagellar motility is often costly[26–28]. Flagellar expression also has a cost in *P. syringae* (Fig. 3 and Extended Data Fig. 4), although this cost is clearer at the single-cell level (Fig. 3e–g). In *Salmonella*, costs linked to expression of SPI1 T3SS have been proposed as a factor favouring both counter-regulation with flagella and maintenance of heterogeneity[24,25]. T3SS expression also carries a growth penalty in *P. syringae* (Fig. 3), and the strong growth advantage of a *ΔfliC ΔhrpL* double mutant indicates an even greater fitness cost associated to expression of both. Phenotypic heterogeneity is considered particularly advantageous when affecting loci producing immunogenic and/or energetically costly goods, with cost to the producers and benefits to the population defining a cooperative behaviour[39–41]. The growth penalties detected for flagellar and T3SS expression in *P. syringae* provide selective advantages to phenotypically heterogeneous populations and may drive selection of genetic and/or epigenetic mechanism(s) underlying such heterogeneities. For bacteria engaging in host interactions, heterogeneous expression lowers the overall amount of flagellin displayed by the population, or by a microcolony at a local level, and could be also advantageous by reducing defence elicitation and facilitating immune suppression.

Cooperative virulence can also prevent the rise of non-producing mutant variants at the expense of the producers[42–45]. Phenotypically OFF bacteria can outcompete less frequent mutant OFF variants and safely revert to ON, thus preventing loss of function and stabilizing the cooperative behavior[43]. Cheater mutant variants affected in type III secretion have been described in *P. syringae* populations colonizing *Arabidopsis*, although at frequencies lower than expected considering the potential for exploitation of T3SS effectors as public goods[22,46].

This role of T3SS effectors as public goods has been reported using mutants[32] and metapopulations, where mixed isogenic *P. syringae* derivatives lacking effectors, and each overexpressing a single effector, cooperatively restore virulence[46].

Phenotypic heterogeneity can also allow bacterial populations to cope with rapid environmental changes, since preexisting subpopulations preadapted to incoming stresses can overcome these changes faster[39,40]. This is known as 'bet-hedging'[41]. Phenotypic heterogeneity can also lead to 'division of labour' when a population diversifies, allowing the distribution of tasks among phenotypically different variants. While in bet-hedging, one subpopulation is fitter than the other in each environment, division of labour increases fitness for the entire population[41]. We found no evidence of any T3SS/flagellar phenotypic variant benefiting during plant colonization, as expected in a bet-hedging scenario. However, different defence elicitation contexts (for example, resistant plants) might differentially benefit certain phenotypes, as shown for genome-reorganized variants[47,48]. Our results support a 'division of labour' scenario, with T3SS^{ON} bacteria complementing T3SS^{OFF} probably through suppressing immunity by 'common goods' T3SS effectors[22] (Fig. 4 and Extended Data Fig. 5). The percentage of T3SS^{ON} bacteria required for effective *trans* complementation of T3SS^{OFF}, since a subpopulation is expressing immunogenic flagellin, is likely to be balanced by growth trade-offs.

As eukaryotic cell types work within tissues, bacterial cooperation emerges within spatially structured populations[49]. However, structured cooperation has been rarely shown within the context of disease[50]. Indeed, although phenotypic heterogeneity is well documented in planktonic cultures, how these processes occur in spatially structured communities is less understood[51]. The regulatory loops involved in establishing bistable expression of the T3SS in planktonic HIM[20] cultures are in place during plant colonization[19,52]. However, apoplastic bacteria encounter different stimuli specific to their microenvironment, which changes over time, potentially leading to cell-to-cell variation orthogonal to that generated through T3SS and flagellar stochastic heterogeneity. Time-course analysis of T3SS and flagellar expression during plant colonization shows heterogeneity throughout time and locations, but also an overlapping structured pattern (Fig. 4). On the leaf surface, most bacteria are T3SS^{OFF} regardless of the single-cell status of flagellar expression, changing to a majority of T3SS^{ON}/ Flagella^{OFF} during early growth in the apoplast (Fig. 4a,b, 1 dpi). From 2 dpi onwards, heterogeneity is the norm for both loci, but predominantly T3SS^{ON} or Flagella^{ON} areas appear. These areas show a three-dimensional (3D) pattern: those closely associated to host-cell surfaces are enriched in T3SS^{ON} bacteria, while distal areas, or the innermost parts of the microcolony, are predominantly Flagella^{ON} (Figs. 4 and Extended Data Fig. 7, and Supplementary Videos 4 and 5). This is consistent with the notion of T3SS^{ON} bacteria predominantly located where T3SS activity is relevant to suppress cellular immunity and explains the lack of selective killing of T3SS^{OFF} bacteria[26] (Extended Data Fig. 5). Such phenotypic differentiation into spatially distributed subpopulations cooperating in a complex environment (that is, in planta vs in vitro) has rarely been investigated, particularly for more than a trait[53], but it is reasonable to expect it to take place in the context of host colonization processes. Spatially structured cooperation in the context of disease has been demonstrated for cholera toxin and toxin-coregulated pilus in *Vibrio cholerae in mice intestinal microcolonies*, and for nitric oxide (NO)-detoxifying *hmp* gene in *Yersinia pseudotuberculosis* in spleen microcolonies[49,53]. Spatial heterogeneity has also been described through single-cell omics within in vitro biofilms of human pathogen *P. aeruginosa*, including variation in flagellar expression[54]. Host-cell signals, cell-to-cell interactions or lineage history[55] could be involved in T3SS activation in host-proximal areas. How environmental signals combine with stochastic processes to generate phenotypic variation is a current topic of interest[55], one particularly challenging to study beyond in vitro systems if positional information is to be obtained[55].

As apoplastic microcolonies develop, Flagella^{ON} bacteria increase in numbers. Motile bacteria are expected to exit the leaf more efficiently (Extended Data Fig. 7), and our results experimentally support this notion by showing that mostly Flagella^{ON} bacteria exit colonized tissue before necrosis (Fig. 5). The final stages of the infection and host exit is an understudied domain, even for model pathogen *P. syringae*, so whether this active early exit is more biologically relevant than passive exit from necrotic tissue remains to be explored, but it appears a safer strategy since necrosis leads to the release of toxic compounds and to the activation of additional defence responses[56,57].

Only a handful of studies have analysed expression of two bistable heterogeneous loci simultaneously[49,53,58]. Ours studies two loci relevant for bacterial–host interaction (Supplementary Video 10) and does it in the context of disease within a spatially structured dynamic microcolony. It provides an example of division of labour and cooperative virulence in a plant host, validating the importance of phenotypic heterogeneity in nature and shifting the emphasis from its mechanistic understanding to its ecological and biological relevance. Finally, the study establishes phenotypic heterogeneity and cooperative virulence as a conserved strategy by which bacterial pathogens cope with the fluctuating challenges encountered in plant and animal hosts.

Methods

Bacterial strains and growth conditions

Bacterial strains used and generated in this work are detailed in Supplementary Table 1. *E. coli and P. syringae* strains were grown with aeration in LB medium[59] at 37 °C for *E. coli* or 28 °C for *P. syringae*. Antibiotics were used, when necessary, at the following concentrations: ampicillin, 100 μg ml^{-1} for *E. coli* and 500 μg ml^{-1} for *P. syringae*; kanamycin, 50 μg ml^{-1} for *E. coli* and 15 μg ml^{-1} for *P. syringae* derivative strains; gentamycin, 10 μg ml^{-1}; nitrofurantoin, 40 μg ml^{-1}; and cycloheximide, 2 μg ml^{-1}.

To induce the expression of the *hrp/hrc* genes, bacteria were initially cultured overnight in LB at 28 °C, supplemented with the appropriate antibiotic, then washed twice in 10 mM $MgCl_2$ before being cultured in *hrp*-inducing minimal medium (HIM), containing 10 mM fructose[60]. For this study, the pH of HIM was adjusted to 7.0 with 10 N NaOH. The initial optical density (OD) was adjusted to 0.13 and cultures were incubated at 28 °C with agitation.

Fluorescence labelling of bacterial strains

Bacterial strains carrying a chromosome-located transcriptional fusion of *fliC* gene to a promoterless *tdTomato* gene were generated using an adaptation of the method previously described in ref. 61. The plasmids used and generated for this purpose are detailed in Supplementary Table 2. The primers used are described in Supplementary Table 3. For the generation of the allelic exchange plasmid, two fragments of ~500 pb were amplified from *Pph* 1448A genomic DNA using Q5 High-Fidelity DNA Polymerase (New England Biolabs); one of these fragments (A) encompasses the 3′ end of the open reading frame (ORF), including the STOP codon, while the other fragment (B) covers the sequence immediately downstream of the STOP codon. All primers used are described in Supplementary Information. Each reaction was carried out at 98 °C for 1 min for the initial denaturation step, followed by 30 cycles at 98 °C for 30 s, annealing at 62 °C for 30 s and extension at 72 °C for 30 s, followed by 5 min at 72 °C for the final extension step. The reaction mixture for each PCR included 0.64 mM deoxynucleotide triphosphate (dNTP) mix, 0.4 ng of each primer, 1 ng of genomic DNA, the appropriate enzyme buffer and commercial ultrapure water (Nalgene). A volume of 2 μl of each gel-purified PCR product was employed as template for the subsequent fusion PCR, employing primers A1 and B2 in a PCR reaction conducted under the conditions described, with an extended elongation time of 1 min. The resulting bands, comprising the end of each ORF and its downstream sequence separated by an *EcoRV* restriction site, were A/T cloned into

pGEM-T (Promega) and subjected to full sequencing to discard clones carrying mutations. This process rendered the pGT-AB-*fliC* plasmid necessary for generating the allelic exchange plasmid.

The sequence of the promoterless *tdTomato* (*tdT*) gene was acquired through PCR amplification from the tdTomato-pBAD plasmid (Addgene plasmid 54856) using the ProtFluorF and ProtFluorR primers. This PCR generated a *tdTomato* fragment with a 5′ *EcoRV* restriction site and a 3′ *EcoRI* restriction site. Similarly, the kanamycin cassette (*nptII*; EJQ5150444.1) was amplified using the P1 EcoRV and P2 EcoRI primers, and plasmid pKD4 served as DNA template to obtain the FRT-*nptII*-FRT fragment needed for the resistance to kanamycin. This fragment featured a 5′ *EcoRV* and 3′ *EcoRI* restriction site. Both amplification reactions were performed using Q5 High-Fidelity DNA Polymerase (New England Biolabs) in a 50-µl PCR reaction mixture consisting of 500 ng of plasmid as DNA template, 0.5 µM of each primer, 0.2 mM dNTPs and 0.5 µl of Q5 High-Fidelity DNA Polymerase. Each reaction followed a thermal cycling protocol that began with an initial step of 98 °C for 2 min, followed by 30 cycles at 98 °C for 10 s, 60 °C for 30 s and 72 °C for 45 s, concluding with a final extension at 72 °C for 5 min. The gel-purified fragments, both the *tdTomato* and the FRT-*nptII*-FRT, underwent digestion with EcoRI and EcoRV enzymes and were cloned into the EcoRV-digested pGT-AB-*fliC* plasmid, rendering the allelic exchange plasmid to be named pGT-*fliC::tdT*.

Strain 1448A *fliC::tdT* was obtained by introducing the pGT-*fliC::tdT* plasmid into *P. syringae* pv. *phaseolicola* 1448A through electroporation, following the method described in ref. 61. Selection was carried out on LB plates with kanamycin. Subsequently, the resulting colonies were replicated onto LB plates with ampicillin (500 µg ml^{-1}) to discard the colonies with plasmid integration, which is indicative of a single recombination event. The colonies that exhibited kanamycin resistance but ampicillin sensitivity were then confirmed through PCR using the A1 *fliC* and B2 *fliC* primers, and through Southern blot analysis employing the *nptII* gene as a probe to confirm proper allelic exchange resulting from a double recombination event occurring at a unique position within the genome. To generate strains carrying two chromosomal transcriptional fusions, the pGT-*fliC::tdT* plasmid was transformed into the previously generated strains 1448A *hrpL::GFP3*, 1448A *hopAB1::GFP3* and 1448A *hrcU::GFP3*, to generate the 1448A *hrpL::GFP3 fliC::tdT*, 1448A *hopAB1::GFP3 fliC::tdT* and 1448A *hrcU::GFP3 fliC::tdT* strains.

Bacterial strains carrying a chromosome-located transcriptional fusion of *fliC* gene to a promoterless *GFP3* gene, 1448A *fliC::GFP3* strains, were generated following a modified method[62]. The *GFP3*-FRT-*nptII*-FRT fragment was obtained by digesting the plasmid pGT-GFP^{+} with the EcoRI digestion enzyme. This fragment consists of the promoterless *GFP3* gene, complete with its ribosomal binding site, followed by the kanamycin resistance gene (*nptII*) flanked by flipase recognition target (FRT) sites, with the entire construct bordered by two *EcoRI* restriction sites. The *GFP3*-FRT-*nptII*-FRT fragment was then blunt ended through a PCR procedure and ligated into *EcoRV*-digested pGT-AB-*fliC* through blunt-end ligation, leading to the generation of the pGT-*fliC::GFP3* plasmid. Subsequently, the resulting plasmid was transformed into *P. syringae* pv. *phaseolicola* 1448A to generate the 1448A *fliC::GFP3* strain.

In addition, the constitutively expressed fluorescent reporter gene *eCFP* was introduced into the chromosome of the 1448A *fliC::GFP3* and 1448A *hopAB1::GFP3 fliC::tdT* strains using a Tn*7* delivery system[23] to generate the 1448A *fliC::GFP3 eCFP* and 1448A *hopAB1::GFP3 fliC::tdT eCFP* strains.

Generation of mutant bacterial strains

The bacterial strain carrying a deletion of the *fleQ* gene was generated following the method described in ref. 61, which involves the generation of gene knockouts by allelic exchange, replacing the specific ORF by a kanamycin cassette. The allelic exchange plasmid pGT-*ΔfleQ* was generated as previously described for the generation of the pGT-AB-*fliC* using primers A1 *ΔfleQ*, A2 *ΔfleQ*, B1 *ΔfleQ* and B2 *ΔfleQ*, and the same experimental settings described above. The FRT-*nptII*-FRT fragment was obtained by PCR amplification using P1 EcoRI and P2 EcoRI primers and pKD4 as template, and the kanamycin cassette was finally inserted by ligation in the *EcoRI* restriction site, generating the allelic exchange plasmid pGT-Δ*fleQ*. This plasmid was transformed into 1448A *Pseudomonas syringae* pv. *phaseolicola* and mutants were obtained as described in ref. 61.

The bacterial strain carrying a deletion of the *hrpL* gene and of the *fliC* gene was generated by allelic exchange as previously described, transforming the plasmid pGT-*ΔfliC* described in ref. 29 into the *ΔhrpL* strain described in ref. 19 to render *ΔhrpL ΔfliC* double-mutant strain.

Generation of pFleQ

pFleQ was generated using the backbone of pBBRMCS-4. For its generation, the *fleQ* ORF was amplified using Q5 High-Fidelity DNA Polymerase (New England Biolabs) in a 50 µl PCR reaction mixture consisting of 500 ng of 1448A *Pseudomonas syringae* genome as DNA template, 0.5 µM of *fleQ*F and *fleQ*R primers, 0.2 mM dNTPs and 0.5 µl of Q5 High-Fidelity DNA Polymerase. The reaction followed a thermal cycling protocol that began with an initial step of 98 °C for 2 min, followed by 30 cycles at 98 °C for 10 s, 60 °C for 30 s and 72 °C for 45 s, concluding with a final extension at 72 °C for 5 min. The gel-purified fragment underwent digestion with KpnI and SacII enzymes, and was cloned into the KpnI/SacII-digested pBBRMCS-4 plasmid. The resulting clones were subjected to full sequencing to discard those carrying mutations, and transformed into the corresponding bacterial strains using the method described in ref. 61 for plasmid transformation of *P. syringae*.

Plant growth and inoculation

Phaseolus vulgaris bean cultivar Canadian Wonder plants were cultivated under controlled conditions at 23 °C and 95% humidity. Artificial light was maintained for periods of 16 h within the 24 h of the day. All experiments carried out were performed using 10-day-old plants.

For the preparation of bacterial inoculum, bacterial lawns were cultivated onto LB plates for 48 h at 28 °C. Subsequently, biomass was resuspended in 2 ml of 10 mM $MgCl_2$. The OD_{600} was adjusted to 0.1, corresponding to the concentration of 5×10^7 colony-forming units per millilitre (c.f.u.s ml^{-1}). Serial dilutions were performed to achieve the desired final inoculum concentration.

The infiltration of bean leaves for visualizing microcolonies using confocal microscopy was performed using a needleless syringe with bacterial suspension at 5×10^5 to 10^6 c.f.u.s ml^{-1}.

The inoculation of bean leaves for visualizing bacteria on the surface using confocal microscopy was performed by dipping. For this, a bacterial suspension with 5×10^7 c.f.u.s ml^{-1} was prepared in a 10 mM $MgCl_2$ solution, and the entire leaf was submerged in the inoculum for a few seconds. Visualization was performed at 6 h post inoculation.

For infiltrating bean leaves to extract bacteria from the apoplast for subsequent analysis by FC and CLSM, a previous report[63] was followed. This involved immersing the entire leaf in a bacterial solution with a concentration of 5×10^4 c.f.u.s ml^{-1}, containing 0.01% Silwett L-77 (Crompton Europe), and using a pressure chamber. Bacteria were recovered from the plant at 4 dpi through apoplastic fluid extraction. This extraction process[63] entailed pressure infiltrating a whole leaf with 10 ml of a 10 mM $MgCl_2$ solution inside a 20-ml syringe. After applying 5 cycles of pressure, the flow-through was collected and transferred to a fresh 50-ml tube. Three hundred microlitres of the flow-through were directly analysed by flow cytometry. Simultaneously, the 50-ml tubes were centrifuged for 30 min at low speed (900 *g*) at 4 °C. The resulting pellets were resuspended into 1 ml of a 10 mM $MgCl_2$ solution and subsequently analysed by microscopy.

To compare flagellar expression in cells mechanically extracted from or naturally exiting leaves, bean leaves were infiltrated with a 5×10^7 (for 1 dpi), 5×10^6 (for 2 dpi) or 5×10^5 c.f.u.s ml^{-1} (for 5 and 7 dpi) bacterial suspension using a pressure chamber, as described above. For natural exit mimicking rain, leaves were sprayed with water every 5 min during a 30-min period, and drops flowing through the leaves were collected in a 50-ml cylinder tube. Bacteria were concentrated by centrifugation at 10,000 *g* for 5 min. For quantification at different timepoints, leaves were detached from the stem by cutting the petiole in the base of the leaf blade at the specified timepoints and incubated for 30 min in a 50-ml tube containing 30 ml of 10 mM $MgCl_2$ to analyse natural exit. Mechanical bacterial extraction from the apoplast was carried out as described above.

Flow cytometry and cell sorting

For HIM cultures, 500 µl of an overnight *P. syringae* LB culture was washed twice in 10 mM $MgCl_2$, added to 4.5 ml of HIM and incubated at 28 °C for 24 h. LB cultures were obtained from an overnight incubation in LB and apoplast-extracted bacterial suspensions were obtained as indicated in the 'Plant growth and inoculation' section. Of the cultures in HIM, LB or in planta, 300 µl were analysed using a BD FACS Verse cytometer (BD Biosciences), and graphs were generated with the Kaluza software (Beckman Coulter; https://www.beckman.es/flow-cytometry/software/kaluza). A minimum of 100,000 events were analysed per sample. FITC-A and PE-A filters were used to visualize GFP and tdTomato signals, respectively. To ensure bleedthrough was not taking place, strains with transcriptional single fusions to *GFP3* and *tdTomato* were analysed with the PE-A and FITC-A filters, respectively, with the observation of fluorescence as the negative control level.

For cell sorting, stationary cultures in LB obtained after an overnight incubation were sorted using a BD FACSAria Fusion flow cytometer (BD Biosciences). Exponential cultures in HIM obtained after 24 h of incubation from 0.13 OD_{600} were sorted using a MoFloTM XDP cytometer (Beckman Coulter). To initiate the process of sorting, gates were drawn to distinguish cells displaying fluorescence levels overlapping with the 1448A non-GFP bacterial population, which served as the negative control, from cells expressing higher GFP levels, as indicated in the corresponding histogram. On the basis of this analysis, 1×10^5 events were sorted for cells expressing higher GFP levels and lower GFP levels. Cells from each gate were collected into separate sterile tubes. After sorting, cells were centrifuged at 12,000 *g* for 10 min, and the resulting pellets were resuspended into 10 mM $MgCl_2$. An aliquot of sorted cells was run again in the cytometer to confirm the differences in expression between the separated populations. Data from cytometry experiments were analysed using Kaluza 2.1 (Beckman Coulter) for further analysis and visualization.

Confocal microscopy

For single-cell visualization of apoplast-extracted bacteria and cultured bacteria, suspensions of 2 µl were deposited over a 0.17-mm coverslip, and an agar-pad square was placed on top of the drop to create a bacterial monolayer[63]. To visualize all cells, bacterial suspensions were stained with FM4-64 (Life Technologies) at 20 µM, and bacterial membranes were visualized with fluorescent light; alternatively, in other cases, bright-field images were included. Images of single-cell bacteria were acquired using the Zeiss LSM880 confocal microscope (Zeiss) using ×100 objectives.

For the visualization of *P. syringae* microcolonies and surface cells, sections of inoculated *P. vulgaris* leaves (~5 mm^2) were carefully excised using a razor blade and mounted on slides in double-distilled H_2O, positioning the lower epidermis towards the objective. A 0.17-mm coverslip was placed over the sample. Images of the leaf mesophyll were taken using the Leica Stellaris 8 confocal microscope (Leica Microsystems) with ×40 objectives.

Filters for wavelength selection were used for the visualization of the following fluorophores (excitation/ emission): eCFP (405 nm/450–500), GFP (488 nm/500–533 nm), FM4-64 (488 nm/604–674 nm), tdTomato (514 nm/570–600) and plant autofluorescence (514/605–670 nm). Image processing was performed using Leica LAS AF (Leica Microsystems) software. To ensure bleedthrough was not taking place, strains with transcriptional single fusions to *GFP3*, *tdTomato* and strains constitutively labelled with *eCFP* were observed under the microscope in the visualization conditions mentioned above, with the observation of no fluorescence. *Z*-series imaging was performed at 1 µm using ×40 objectives.

Time-lapse microscopy

Heterogeneous flagellum expression was measured during microcolony formation in HIM + 1.25% agarose pads as follows: 2× HIM medium was mixed with a melted 2.5% agarose solution and immediately placed in the wells of a custom 3D-printed mould (template available at https://github.com/JLuneau/Pseudomonas_AgarPads_fliC/tree/main/3D_printed_AgarPad_mold) disposed on a 50-mm round coverslip (Epredia, CB005005A140MNZ0). To ensure the flatness of the pads, another coverslip was immediately placed on top of the mould. The pads were solidified for 15 min at room temperature. The bottom coverslip was removed and 4 µl of bacterial suspensions adjusted to OD = 0.005 in HIM were dropped on the pad surface. Immediately after the droplets dried, a new coverslip was placed on the mould and the assembled device was mounted on the microscope. For time-lapse experiments, images were taken every 15 min, starting at 4 h after cells were placed on the pads and for 24 h at 25 °C. Images were acquired using the NIS-Elements software on a Nikon Eclipse Ti2 inverted microscope equipped with a Hamamatsu ORCA-Flash4.0LT digital camera and a Nikon Plan Apo Lambda ×100/1.45 oil objective. The 1.5× manual knob was engaged to enhance magnification. Illumination settings: phase contrast, 100 ms, 50% intensity; GFP (470 nm excitation and 519 nm emission filters), 300 ms, 50% intensity. All imaging data are available at https://www.ebi.ac.uk/biostudies/bioimages/studies/S-BIAD1413.

Time-lapse image analysis

Time-lapse movies were visually inspected using Fiji 2.14.0 to crop the region of interest around microcolonies and to remove later frames when cells overlapped. Cells were segmented and tracked using the DeLTA 2.0 deep learning-based pipeline[64] with the default pretrained models for segmentation and tracking. Time-lapse data analysis was performed using custom Python scripts adapted from ref. 65 (available at https://github.com/JLuneau/Pseudomonas_AgarPads_fliC). Visual inspection of DeLTA 2.0 output movies showed that while segmentation errors were rare, tracking errors were frequent at late timepoints. Thus, similarly to ref. 65, we filtered out erroneous cell tracks. Upon division, (1) we kept cells for which two sister cells were tracked for at least four frames after division, (2) we excluded sister cells for which the cumulated length at birth differed strongly from the length of the mother cell before division (increase or decrease of more than 20%) and (3) we excluded sister cells that showed unexpectedly large jumps in cell length between two frames (increase or decrease of more than 20%). For all retained cells, the *fliC* expression level was estimated as the mean fluorescence intensity in the GFP channel for all pixels belonging to a single cell, averaged over the lifetime of each individual cell. The growth rate was obtained by performing a linear regression on the log-transformed cell length over the lifetime of each cell. To estimate the cost of flagellum expression, we grouped cells into two classes: the GFP-high cells showing a mean fluorescence intensity above the median fluorescence intensity of all cells, and the GFP-low cells showing a mean fluorescence intensity below the population's median.

Live/dead staining

One drop of the propidium iodide solution Ready Probes (Thermo Fisher) was added to 300 µl of the suspension with apoplast-extracted

bacteria, and live/dead bacteria were identified by flow cytometry. For live/dead staining, bacteria were syringe infiltrated into bean leaves at 5×10^4 c.f.u.s ml^{-1} and extracted from the apoplast at 4 dpi.

Competitive index assay

CI was calculated by determining the ratio between the mutant strain and the wild type in the output sample divided by that in the input (which should be 1.0)[66]. Assays were performed after the mixed strains had been growing in either bean leaves or LB and HIM cultures.

CI assays[66] were performed in bean plants (*Phaseolus vulgaris* cv. Canadian wonder). Bean plants were inoculated with 200 µl of a mixed bacterial suspension containing 5×10^4 c.f.u.s ml^{-1} of each strain, consisting of an equal proportion of wild type and mutant strains. For the assay performed in Fig. 3d, the peptide flg22 (GeneScript) was added to the bacterial suspension to a 100 nM concentration. Inoculation was performed using a 1-ml syringe without needle. Samples were extracted for quantification at 4 dpi. Bacterial recovery was carried out by taking 5 discs of 1-cm diameter from the infected leaf with a cork borer and homogenizing them by mechanical disruption into 1 ml of 10 mM $MgCl_2$. After homogenization, serial dilutions of the bacterial suspensions were prepared and plated onto agar plates supplemented with 2 µg ml^{-1} cycloheximide. Bacterial enumeration was performed and CIs were calculated after 2 days of growth at 28 °C. To distinguish wild-type from mutant bacteria within the mixed infection, an aliquot from the same dilution was plated onto LB agar and LB agar plates supplemented with kanamycin.

For CI assays performed in LB cultures, 500 µl of a mixed bacterial suspension with 5×10^5 c.f.u.s ml^{-1} was inoculated into 4,500 µl of liquid LB in culture tubes. For CI assays performed in HIM cultures, 500 µl of a mixed bacterial suspension with 5×10^7 c.f.u.s ml^{-1} was inoculated into 4,500 µl of liquid LB in culture tubes. After 24 h of incubation with continuous agitation, in both LB or HIM cultures, serial dilutions were prepared and plated onto LB agar and LB agar plates supplemented with kanamycin.

To confirm dosage and relative proportion of the strains, serial dilutions of the inocula were plated onto LB agar and LB agar plates supplemented with the appropriate antibiotic. After bacterial counting, the ratio of the wild-type vs the mutant strain should be close to 1. The competitive indices represent the mean of at least three independent experiments, each with at least three replicates each. Error bars indicate standard error. Statistical analysis was performed using two-tailed Student's *t*-test with a significance threshold of $P < 0.05$ to assess deviations from a ratio of 1.

In vitro growth curves

Growth curves to analyse growth differences between mutant and overexpressing strains were generated by culturing strains in 96-well plates (Biofil), adjusting the bacterial inoculum to an optical density (Abs_{600}) of 0.13 in HIM in 150 µl of final volume. The inoculum was obtained from an overnight LB culture and cells were washed twice with $MgCl_2$ before adjusting the optical density. Plates were incubated for 50 h at 28 °C with agitation in an EONC plate reader (Bio Tek Instruments).

Growth curves to compare *ΔhrpL* growth vs that of the wild-type strain were generated by culturing strains in culture tubes in HIM at an initial optical density of 0.13 (Abs_{600}). The inoculum was obtained from an overnight culture in LB, washed twice with $MgCl_2$. Samples were taken at 20, 24, 26, 28, 30, 34, 38, 44, 48 and 50 h.

To calculate bacterial growth rate, the $\log_{10}$ of absorbance data were calculated and represented versus time. The regression curve was calculated over the zone of exponential growth and the graph slope obtained was used as the growth rate.

Flagellar motility assay

Flagellar motility assays were conducted after sorting bacterial cultures carrying *fliC::GFP3* by inoculating 2 µl of the aliquots obtained after sorting (adjusted to 10,000 sorting events) in HIM plates containing 2.5 g l^{-1} agar or in tryptone plates containing 3% tryptone, 5% $MgCl_2$ and 2.5 g l^{-1} agar. Plates were subsequently incubated at 28 °C, and digital photographs were captured to measure the diameter of the swimming halo. Images were then taken at 1 and 3 dpi (for LB-grown sorted samples) or 3 dpi (for HIM-grown sorted samples). Halos obtained were measured and the ratio between the diameters of high versus low expression within each sorted pair was calculated.

Quantification, statistical analysis and reproducibility

All quantification and statistical analysis described in this study was performed using GraphPad Prism 9.0 (Prism; https://www.graphpad.com/). Details of the analysis used and specific *P* values are indicated in the figure legends for each experiment, for all or at least significantly different values. Reproducibility was tested in independent experiments and the total number of biological replicates indicated in figure legends. Software used for data quantification and analysis are further detailed in Supplementary Table 4. In all scatterplot graphs, mean ± s.e.m. are indicated. No statistical method was used to predetermine sample size. No data were excluded from the analyses, except for Figs. 1a and 5b, and Extended Data Fig. 6b,c in which, to adjust the sample size (*n* value) between conditions, some data were excluded following blind elections. The experiments were not randomized. The investigators were not blinded to allocation during experiments and outcome assessment.

Reporting summary

Further information on research design is available in the Nature Portfolio Reporting Summary linked to this article.

Data availability

All data generated has been made available in the public repository Zenodo and the DOIs generated for each figure and extended data figure listed in refs. 67–77. Source data are provided with this paper.

Code availability

Time-lapse data analysis was performed using custom Python scripts adapted from ref. 65 (https://github.com/JLuneau/Pseudomonas_AgarPads_fliC). This paper does not report original code. Any additional information required to reanalyse the data reported in this work is available from the lead contact upon request.

References

1. Morris, C. E., Monteil, C. L. & Berge, O. The life history of *Pseudomonas syringae:* linking agriculture to earth system processes. *Annu. Rev. Phytopathol.* https://doi.org/10.1146/annurev-phyto-082712-102402 (2013).
2. Haefele, D. M. & Lindow, S. E. Flagellar motility confers epiphytic fitness advantages upon *Pseudomonas syringae*. *Appl. Environ. Microbiol.* **53**, 2528–2533 (1987).
3. Panopoulos, N. J. Role of flagellar motility in the invasion of bean leaves by *Pseudomonas phaseolicola*. *Phytopathol.* https://doi.org/10.1094/Phyto-64-1389 (1974).
4. Ichinose, Y., Taguchi, F. & Mukaihara, T. Pathogenicity and virulence factors of *Pseudomonas syringae*. *J. Gen. Plant Pathol.* **79**, 285–296 (2013).
5. DeFalco, T. A. & Zipfel, C. Molecular mechanisms of early plant pattern-triggered immune signaling. *Mol. Cell* **81**, 3449–3467 (2021).
6. Yu, X. et al. Transcriptional responses of *Pseudomonas syringae* to growth in epiphytic versus apoplastic leaf sites. *Proc. Natl Acad. Sci. USA* https://doi.org/10.1073/pnas.1221892110 (2013).
7. Nobori, T. et al. Transcriptome landscape of a bacterial pathogen under plant immunity. *Proc. Natl Acad. Sci. USA* https://doi.org/10.1073/pnas.1800529115 (2018).

8. Nobori, T. et al. Multidimensional gene regulatory landscape of a bacterial pathogen in plants. *Nat. Plants* **6**, 883–896 (2020).
9. Cummings, L. A., Wilkerson, W. D., Bergsbaken, T. & Cookson, B. T. In vivo, *fliC* expression by *Salmonella enterica* serovar Typhimurium is heterogeneous, regulated by ClpX, and anatomically restricted. *Mol. Microbiol.* **61**, 795–809 (2006).
10. Saini, S., Ellermeier, J. R., Slauch, J. M. & Rao, C. V. The role of coupled positive feedback in the expression of the SPI1 type three secretion system in *Salmonella*. *PLoS Pathog.* **6**, e1001025 (2010).
11. Koirala, S. et al. A nutrient-tunable bistable switch controls motility in *Salmonella enterica* serovar Typhimurium. *mBio* https://doi.org/10.1128/mBio.01611-14 (2014).
12. Zarkani, A. A. et al. *Salmonella* heterogeneously expresses flagellin during colonization of plants. *Microorganisms* **8**, 815 (2020).
13. Wang, X., Koirala, S., Aldridge, P. D. & Rao, C. V. Two tandem mechanisms control bimodal expression of the flagellar genes in *Salmonella enterica*. *J. Bacteriol*. https://doi.org/10.1128/JB.00787-19 (2020).
14. Leal-Morales, A., Pulido-Sánchez, M., López-Sánchez, A. & Govantes, F. Transcriptional organization and regulation of the *Pseudomonas putida* flagellar system. *Environ. Microbiol.* **24**, 137–157 (2022).
15. Nogales, J. et al. FleQ coordinates flagellum-dependent and -independent motilities in *Pseudomonas syringae* pv. tomato DC3000. *Appl. Environ. Microbiol.* **81**, 7533–7545 (2015).
16. Schreiber, K. J., Chau-Ly, I. J. & Lewis, J. D. What the wild things do: mechanisms of plant host manipulation by bacterial type III-secreted effector proteins. *Microorganisms* **9**, 1029 (2021).
17. Fouts, D. E. et al. Genomewide identification of *Pseudomonas syringae* pv. tomato DC3000 promoters controlled by the HrpL alternative sigma factor. *Proc. Natl Acad. Sci. USA* **99**, 2275–2280 (2002).
18. Preston, G., Deng, W.-L., Huang, H.-C. & Collmer, A. Negative regulation of *hrp* genes in *Pseudomonas syringae* by HrpV. *J. Bacteriol.* **180**, 4532–4537 (1998).
19. Ortiz-Martín, I., Thwaites, R., Macho, A. P., Mansfield, J. W. & Beuzón, C. R. Positive regulation of the hrp type III secretion system in *Pseudomonas syringae* pv. *phaseolicola*. *Mol. Plant Microbe Interact.* **23**, 665–681 (2010).
20. Rufián, J. S. et al. *Pseudomonas syringae* differentiates into phenotypically distinct subpopulations during colonization of a plant host. *Environ. Microbiol.* **18**, 3593–3605 (2016).
21. Mansfield, J. et al. Top 10 plant pathogenic bacteria in molecular plant pathology. *Mol. Plant Pathol.* **13**, 614–629 (2012).
22. Rufián, J. S. et al. Confocal microscopy reveals in planta dynamic interactions between pathogenic, avirulent and non-pathogenic *Pseudomonas syringae* strains. *Mol. Plant Pathol.* **19**, 537–551 (2018).
23. López-Pagán, N., Rufián, J. S., Ruiz-Albert, J. & Beuzón, C. R. Dual-fluorescence chromosome-located labeling system for accurate in vivo single-cell gene expression analysis in *Pseudomonas syringae*. *Methods Mol. Biol.* **2751**, 95–114 (2024).
24. Sturm, A. et al. The cost of virulence: retarded growth of *Salmonella typhimurium* cells expressing type III secretion system 1. *PLoS Pathog.* **7**, e1002143 (2011).
25. Sánchez-Romero, M. A. & Casadesús, J. Contribution of SPI-1 bistability to *Salmonella enterica* cooperative virulence: insights from single cell analysis. *Sci. Rep.* **8**, 14875 (2018).
26. Macnab, R. in *Escherichia Coli and Salmonella: Cellular and Molecular Biology* 2nd edn (eds Neidhardt, F. C. & Curtiss, R.) 119–130 (ASM Press, 1996).
27. Martínez-García, E., Nikel, P. I., Chavarría, M. & de Lorenzo, V. The metabolic cost of flagellar motion *Pseudomonas putida* KT2440. *Environ. Microbiol.* **16**, 291–303 (2014).
28. Schavemaker, P. E. & Lynch, M. Flagellar energy costs across the tree of life. *eLife* **11**, e77266 (2022).
29. Leba, L. et al. CML9, an *Arabidopsis* calmodulin-like protein, contributes to plant innate immunity through a flagellin-dependent signalling pathway. *Plant J.* **71**, 976–989 (2012).
30. Lehtinen, J., Nuutila, J. & Lilius, E. Green fluorescent protein–propidium iodide (GFP–PI) based assay for flow cytometric measurement of bacterial viability. *Cytometry A* **60A**, 165–172 (2004).
31. Patel, R. R., Kandel, P. P., Traverso, E., Hockett, K. L. & Triplett, L. R. *Pseudomonas syringae* pv. *phaseolicola* uses distinct modes of stationary-phase persistence to survive bacteriocin and streptomycin treatments. *mBio* https://doi.org/10.1128/mBio.00161-21 (2021).
32. Ackermann, M. et al. Self-destructive cooperation mediated by phenotypic noise. *Nature* **454**, 987–990 (2008).
33. Roine, E. et al. Hrp pilus: an hrp-dependent bacterial surface appendage produced by *Pseudomonas syringae* pv. tomato DC3000. *Proc. Natl Acad. Sci. USA* **94**, 3459–3464 (1997).
34. Vargas, P. et al. Plant flavonoids target *Pseudomonas syringae* pv. tomato DC3000 flagella and type III secretion system. *Environ. Microbiol. Rep.* **5**, 841–850 (2013).
35. Freed, N. E. et al. A simple screen to identify promoters conferring high levels of phenotypic noise. *PLoS Genet.* **4**, e1000307 (2008).
36. Sánchez-Romero, M. A. & Casadesús, J. Single cell analysis of bistable expression of pathogenicity island 1 and the flagellar regulon in *Salmonella enterica*. *Microorganisms* **9**, 210 (2021).
37. Wei, C.-F., Deng, W.-L. & Huang, H.-C. A chaperone-like HrpG protein acts as a suppressor of HrpV in regulation of the *Pseudomonas syringae* pv. syringae type III secretion system. *Mol. Microbiol.* **57**, 520–536 (2005).
38. Wei, W. et al. The gene coding for the Hrp pilus structural protein is required for type III secretion of Hrp and Avr proteins in *Pseudomonas syringae* pv. *tomato*. *Proc. Natl Acad. Sci. USA* **97**, 2247–2252 (2000).
39. Fraser, D. & Kærn, M. A chance at survival: gene expression noise and phenotypic diversification strategies. *Mol. Microbiol.* **71**, 1333–1340 (2009).
40. Kamino, K., Keegstra, J. M., Long, J., Emonet, T. & Shimizu, T. S. Adaptive tuning of cell sensory diversity without changes in gene expression. *Sci. Adv.* **6**, eabc1087 (2020).
41. Ackermann, M. A functional perspective on phenotypic heterogeneity in microorganisms. *Nat. Rev. Microbiol.* **13**, 497–508 (2015).
42. Griffin, A. S., West, S. A. & Buckling, A. Cooperation and competition in pathogenic bacteria. *Nature* **430**, 1024–1027 (2004).
43. Diard, M. et al. Stabilization of cooperative virulence by the expression of an avirulent phenotype. *Nature* **494**, 353–356 (2013).
44. Davis, K. M. For the greater (bacterial) good: heterogeneous expression of energetically costly virulence factors. *Infect. Immun*. https://doi.org/10.1128/IAI.00911-19 (2020).
45. Barrett, L. G., Bell, T., Dwyer, G. & Bergelson, J. Cheating, trade-offs and the evolution of aggressiveness in a natural pathogen population. *Ecol. Lett.* **14**, 1149–1157 (2011).
46. Ruiz-Bedoya, T., Wang, P. W., Desveaux, D. & Guttman, D. S. Cooperative virulence via the collective action of secreted pathogen effectors. *Nat. Microbiol.* **8**, 640–650 (2023).
47. Lovell, H. C. et al. In planta conditions induce genomic changes in *Pseudomonas syringae* pv. *phaseolicola*. *Mol. Plant Pathol.* **12**, 167–176 (2011).
48. Neale, H. C. et al. A low frequency persistent reservoir of a genomic island in a pathogen population ensures island survival and improves pathogen fitness in a susceptible host. *Environ. Microbiol.* **18**, 4144–4152 (2016).

49. Davis, K. M., Mohammadi, S. & Isberg, R. R. Community behavior and spatial regulation within a bacterial microcolony in deep tissue sites serves to protect against host attack. *Cell Host Microbe* **17**, 21–31 (2015).
50. Spratt, M. R. & Lane, K. Navigating environmental transitions: the role of phenotypic variation in bacterial responses. *mBio* **13**, e0221222 (2022).
51. Schreiber, F. & Ackermann, M. Environmental drivers of metabolic heterogeneity in clonal microbial populations. *Curr. Opin. Biotechnol.* **62**, 202–211 (2020).
52. Ortiz-Martín, I., Thwaites, R., Mansfield, J. W. & Beuzón, C. R. Negative regulation of the Hrp type III secretion system in *Pseudomonas syringae* pv. *phaseolicola*. *Mol. Plant Microbe Interact.* **23**, 682–701 (2010).
53. Nielsen, A. T. et al. A bistable switch and anatomical site control *Vibrio cholerae* virulence gene expression in the intestine. *PLoS Pathog.* **6**, e1001102 (2010).
54. Dar, D., Dar, N., Cai, L. & Newman, D. K. Spatial transcriptomics of planktonic and sessile bacterial populations at single-cell resolution. *Science* **373**, eabi4882 (2021).
55. van Vliet, S. et al. Spatially correlated gene expression in bacterial groups: the role of lineage history, spatial gradients, and cell–cell interactions. *Cell Syst.* **6**, 496–507.e6 (2018).
56. Zhou, F. et al. Co-incidence of damage and microbial patterns controls localized immune responses in roots. *Cell* **180**, 440–453. e18 (2020).
57. Jacob, P., Hige, J. & Dangl, J. L. Is localized acquired resistance the mechanism for effector triggered disease resistance in plants? *Nat. Plants* **9**, 1184–1190 (2023).
58. Sánchez-Romero, M. A., Olivenza, D. R., Gutiérrez, G. & Casadesús, J. Contribution of DNA adenine methylation to gene expression heterogeneity in *Salmonella enterica*. *Nucleic Acids Res.* **48**, 11857–11867 (2020).
59. Bertani, G. Studies on lysogenesis I. *J. Bacteriol.* **62**, 293–300 (1951).
60. Huynh, T. V., Dahlbeck, D. & Staskawicz, B. J. Bacterial blight of soybean: regulation of a pathogen gene determining host cultivar specificity. *Science* **245**, 1374–1377 (1989).
61. Zumaquero, A., Macho, A. P., Rufián, J. S. & Beuzón, C. R. Analysis of the role of the type III effector inventory of *Pseudomonas syringae* pv. *phaseolicola* 1448a in interaction with the plant. *J. Bacteriol.* **192**, 4474–4488 (2010).
62. Rufián, J. S. et al. in *Methods in Molecular Biology* (eds Medina, C. & López-Baena, F.) 183–199 (Humana Press2018).
63. Rufián, J. S., López-Pagán, N., Ruiz-Albert, J. & Beuzón, C. R. Single-cell analysis of the expression of *Pseudomonas syringae* genes within the plant tissue. *J. Vis. Exp.* https://doi.org/10.3791/64614 (2022).
64. O'Connor, O. M., Alnahhas, R. N., Lugagne, J.-B. & Dunlop, M. J. DeLTA 2.0: a deep learning pipeline for quantifying single-cell spatial and temporal dynamics. *PLoS Comput. Biol.* **18**, e1009797 (2022).
65. Kaczmarczyk, A. et al. A genetically encoded biosensor to monitor dynamic changes of c-di-GMP with high temporal resolution. *Nat. Commun.* **15**, 3920 (2024).
66. Macho, A. P., Zumaquero, A., Ortiz-Martín, I. & Beuzón, C. R. Competitive index in mixed infections: a sensitive and accurate assay for the genetic analysis of *Pseudomonas syringae*–plant interactions. *Mol. Plant Pathol.* **8**, 437–450 (2007).
67. López-Pagán, N., Ruiz-Albert, J. & Beuzón, C. R. Lopez_Pagan_et_al_Nature_Micro_fig_1. *Zenodo* https://doi.org/10.5281/zenodo.14870947 (2025).
68. López-Pagán, N., Ruiz-Albert, J. & Beuzón, C. R. Lopez_Pagan_et_al_Nature_Micro_fig_2. *Zenodo* https://doi.org/10.5281/zenodo.14865081 (2025).
69. López-Pagán, N., Luneau, J., Ruiz-Albert, J. & Beuzón, C. R. Lopez_Pagan_et_al_Nature_Micro_fig_3. *Zenodo* https://doi.org/10.5281/zenodo.14865104 (2025).
70. Rufián, J. S., Ruiz-Albert, J.& Beuzón, C. R. Lopez_Pagan_et_al_Nature_Micro_fig_4. *Zenodo* https://doi.org/10.5281/zenodo.14849825 (2025).
71. Rufián, J. S., Ruiz-Albert, J.& Beuzón, C. R. Lopez_Pagan_et_al_Nature_Micro_fig_5. *Zenodo* https://doi.org/10.5281/zenodo.14849873 (2025).
72. López-Pagán, N., Ruiz-Albert, J. & Beuzón, C. R. Lopez_Pagan_et_al_Nature_Micro_Extended_data_fig_1_V2. *Zenodo* https://doi.org/10.5281/zenodo.14844995 (2025).
73. López-Pagán, N., Ruiz-Albert, J. & Beuzón, C. R. Lopez_Pagan_et_al_Nature_Micro_Extended_data_fig_2. *Zenodo* https://doi.org/10.5281/zenodo.14849770 (2025).
74. López-Pagán, N., Rufián, J. S., Ruiz-Albert, J. & Beuzón, C. R. Lopez_Pagan_et_al_Nature_Micro_Extended_data_fig_3_V2. *Zenodo* https://doi.org/10.5281/zenodo.14865026 (2025).
75. López-Pagán, N., Luneau, J., Ruiz-Albert, J. & Beuzón, C. R. Lopez_Pagan_et_al_Nature_Micro_Extended_data_fig_4_V2. *Zenodo* https://doi.org/10.5281/zenodo.14865041 (2025).
76. López-Pagán, N., Ruiz-Albert, J. & Beuzón, C. R. Lopez_Pagan_et_al_Nature_Micro_Extended_data_fig_5. *Zenodo* https://doi.org/10.5281/zenodo.14865061 (2025).
77. Rufián, J. S., Ruiz-Albert, J. & Beuzón, C. R. Lopez_Pagan_et_al_Nature_Micro_Extended_data_fig_6. *Zenodo* https://doi.org/10.5281/zenodo.14849810 (2025).

Acknowledgements

We thank A. Zumaquero for technical assistance, I. Ortiz-Martín for contribution to preliminary experiments, E. Ruiz-Beuzón for assistance in the final stages of manuscript preparation, S. Ruiz-Beuzón for help with drawing Fig. 4a and A. García, scientific illustrator from Bio-Graphics, for help with Fig. 4c,e,g and Extended Data Fig. 7. This work was supported by project grant PID2021-127245OB-I00 awarded to C.R.B. and J.R.-A., financed by MCIN/AEI/10.13039/501100011033/ and 'ERDP A way of making Europe'. N.L.-P. received funding for a Short-Term Training Mission from COST ACTION SUSTAIN FA1208, supported by COST (European Cooperation in Science and Technology), FEMS research and training grant, and EMBO Scientific Exchange Grant. J.S.R. was supported by Plan Andaluz de Investigación, Desarrollo e Innovación (PAIDI 2020). J.S.L. and S.v.V. were supported by the Swiss National Science Foundation (SNSF) through the Swiss National Centre of Competence in Research (NCCR) Microbiomes (grant number 51NF40_225148) and through an Ambizione Fellowship to S.v.V. (grant number: PZ00P3_202186). L.A. was funded by Aix-Marseille University (AMU) and the Centre National de la Recherche Scientifique (CNRS). M.-A.S.-R. was supported by PID2020-116995RB-I00 funded by MCIN/AEI/10.13039/5011100011033, and CNS2022-135641 funded by MICIU/AEI/10.13039/5011100011033, awarded to M.-A.S.-R., and by the European Union NextGenerationEU/PRTR. We also acknowledge the financial support of the Proyecto QUAL21 012 IHSM, Consejería de Universidad, Investigación e Innovación, Junta de Andalucía, and Universidad de Málaga'.

Author contributions

N.L.-P., J.S.R., J.R.-A. and C.R.B. conceptualized the project. N.L.-P., J.S.R., L.A., M.-A.S.-R., J.L. and S.v.V. developed methodology and software and performed analysis. N.L.-P., J.S.R., J.L., M.-A.S.-R., J.R.-A. and C.R.B. procured resources. C.R.B. wrote the original draft. C.R.B., N.L.-P., J.S.R., J.L., M.-A.S.-R., L.A., S.v.V. and J.R.A. reviewed and edited the manuscript. C.R.B., J.R.-A., J.S.R., N.L.-P., M.-A.S.-R., L.A. and S.v.V. acquired funding. All authors discussed the results and approved the manuscript.

Competing interests
The authors declare no competing interests.

Additional information
Extended data is available for this paper at https://doi.org/10.1038/s41564-025-01966-0.

Supplementary information The online version contains supplementary material available at https://doi.org/10.1038/s41564-025-01966-0.

Correspondence and requests for materials should be addressed to Carmen R. Beuzón.

Peer review information *Nature Microbiology* thanks Andreas Diepold, Bradley Laflamme and the other, anonymous, reviewer(s) for their contribution to the peer review of this work. Peer reviewer reports are available.

https://doi.org/10.1038/s41564-025-01966-0

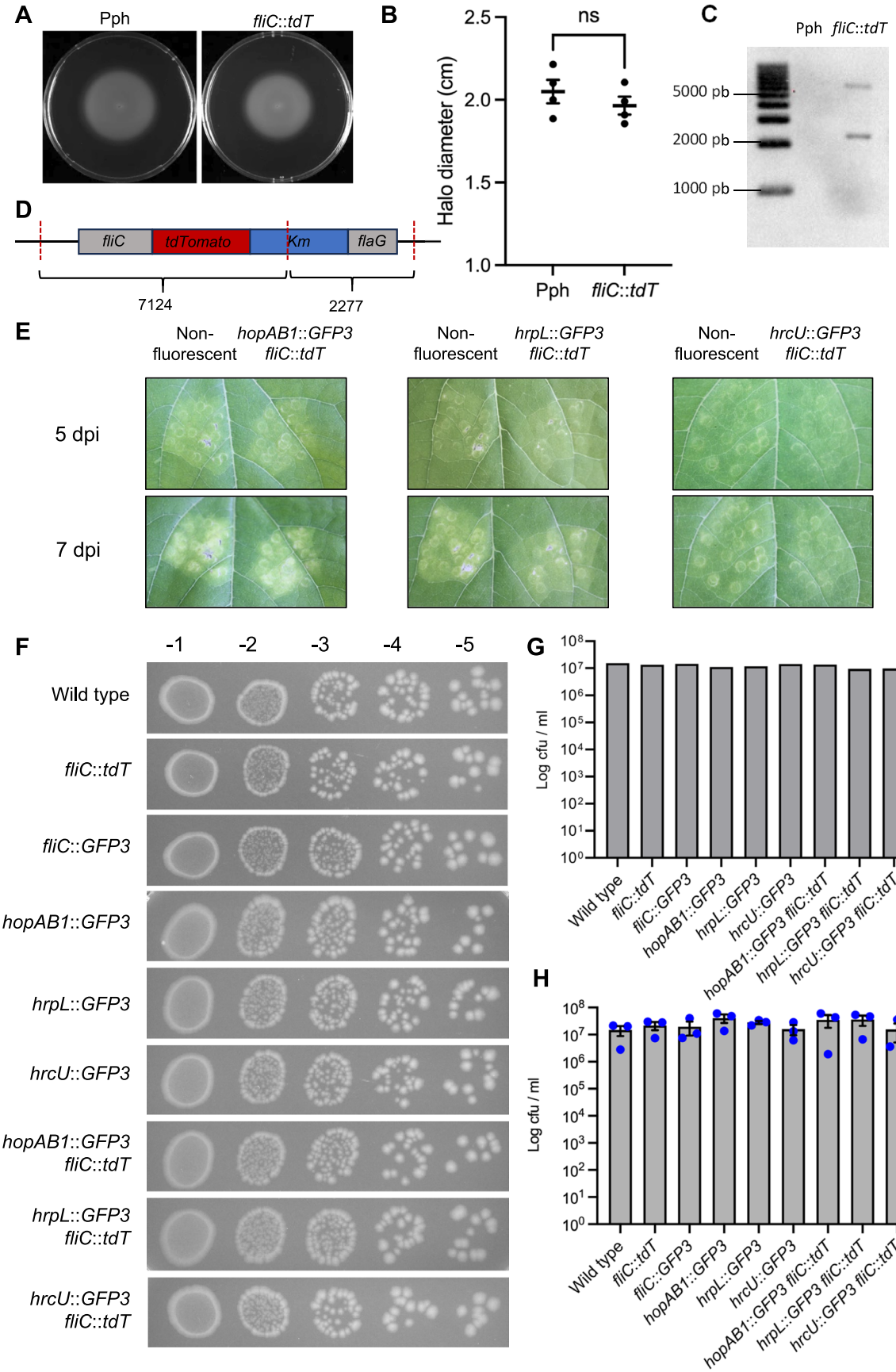

Extended Data Fig. 1 | See next page for caption.

https://doi.org/10.1038/s41564-025-01966-0

Extended Data Fig. 1 | Transcriptional fusions to tdTomato do not affect gene function. (**a**) A strain carrying a *fliC*::*tdT* transcriptional fusion displays wild type motility in the photographs (**a**) and quantifications (**b**) of swimming plates (n = 4). No statistical differences were observed as indicated by an unpaired two-tailed t test ($P < 0.05$). Scatter dot graph shown mean +/− SEM. The *fliC*::*tdT* construct is integrated in the native chromosome location of the *fliC* gene as established by Southern blot analysis (using the *nptII* gene conferring resistance to Km as a probe) of a AlwI21I (Thermo Fisher Scientific, USA) digestion of genomic DNA from the wild type (Pph) and *fliC*::*tdT* derivative strains (**c**) showing the expected band sizes (**d**). (**e**) Representative images of the symptoms caused by the wild type strains and their relative *hopAB1*::*GFP3fliC*::*tdT*, *hrpL*::*GFP3 fliC*::*tdT* and *hrcU*::*GFP3fliC*::*tdT* strains at 5 and 7 dpi. (**f**) Representative images of the colonies obtained after plating serial dilutions of the indicated strains previously adjusted to 0.1 optical density (Abs_{600}). (**g**) Quantification of the data obtained in **f**. All dilutions reach similar values indicating no differences in CFU/ml occasioned by expression of fluorescence reporter genes. **f** and **g** illustrate one experiment (>3 technical replicates), data from 3 additional independent experiments carried out in the same manner are showed in **h**. (**h**) Mean number of cfu/ml obtained after plating a dilution of the culture previously adjusted to 0.1 optical density (Abs_{600}). Data obtained for the different strains (n = 3 biological replicates; technical replicates not used for statistical analysis) did not show significative differences according to a one-way ANOVA followed by Tukey's multiple comparison test ($P < 0.05$). Graph shows individual values (scatter plot) and mean +/− SEM is also indicated.

https://doi.org/10.1038/s41564-025-01966-0

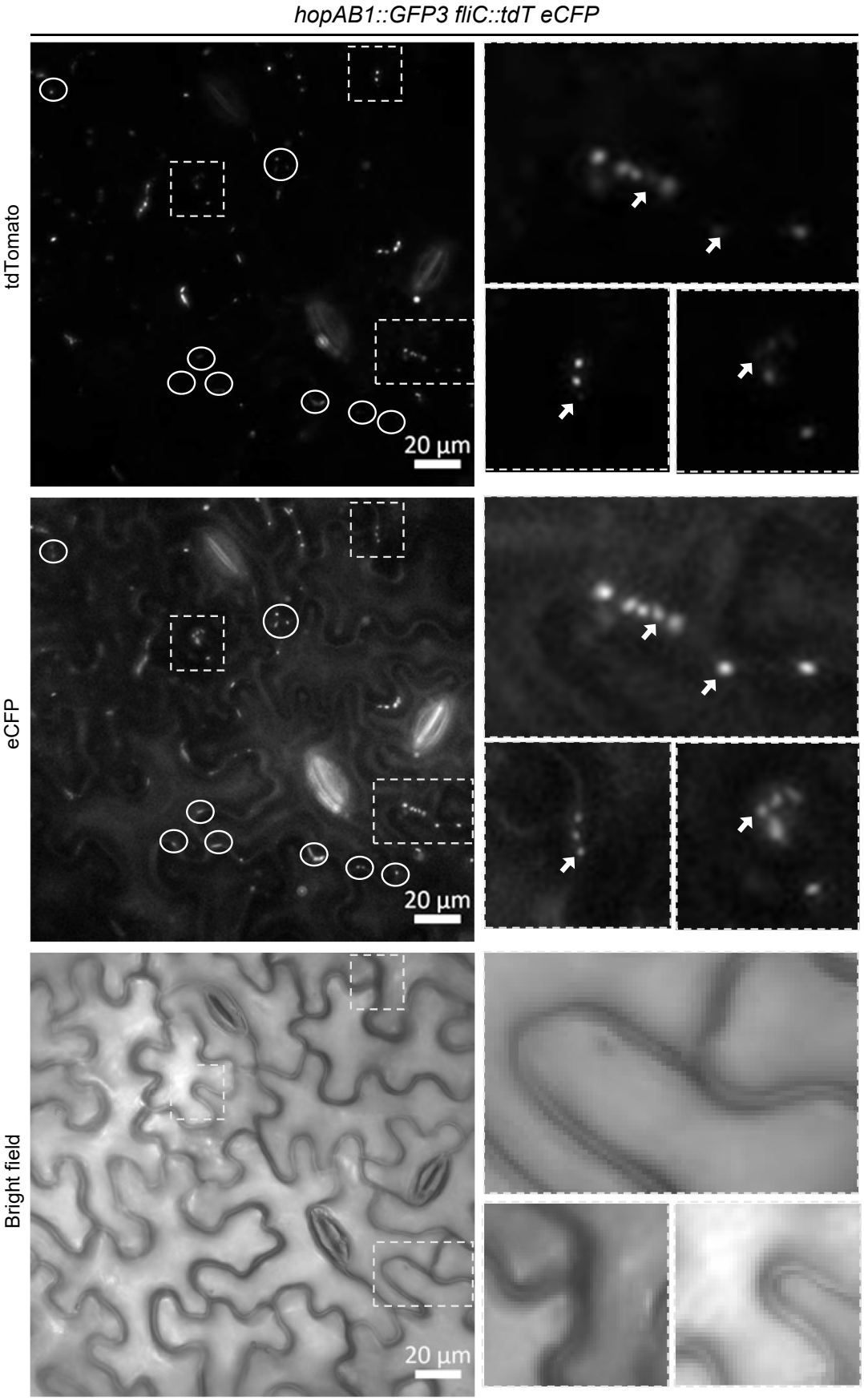

Extended Data Fig. 2 | See next page for caption.

https://doi.org/10.1038/s41564-025-01966-0

Extended Data Fig. 2 | Flagella expression is heterogeneous on plant surface. Selected images of the *hopAB1*::*GFP3 fliC*::*tdT eCFP* strain on the plant surface at 6 h post inoculation (hpi) by dipping the leaf into a 5×10^7 CFU/ml bacterial suspension. tdTomato panel shows the fluorescence of tdTomato associated to *fliC* expression, and eCFP panel shows the fluorescence of eCFP as constitutive expression reporter, using grey scale in both cases to improve contrast. The GFP panel, corresponding to *hopAB1* expression, is not shown since no fluorescence was detected. Scale bars correspond to 20 µm. Contrast and brightness were adjusted to improve visualization but were kept constant across panels. Circles highlight bacteria detected in the eCFP panel without expression in the tdTomato channel (Flagella^{OFF}). Right panels correspond to the magnification of the area selected in rectangles. Images are representative of 3 independent experiments.

https://doi.org/10.1038/s41564-025-01966-0

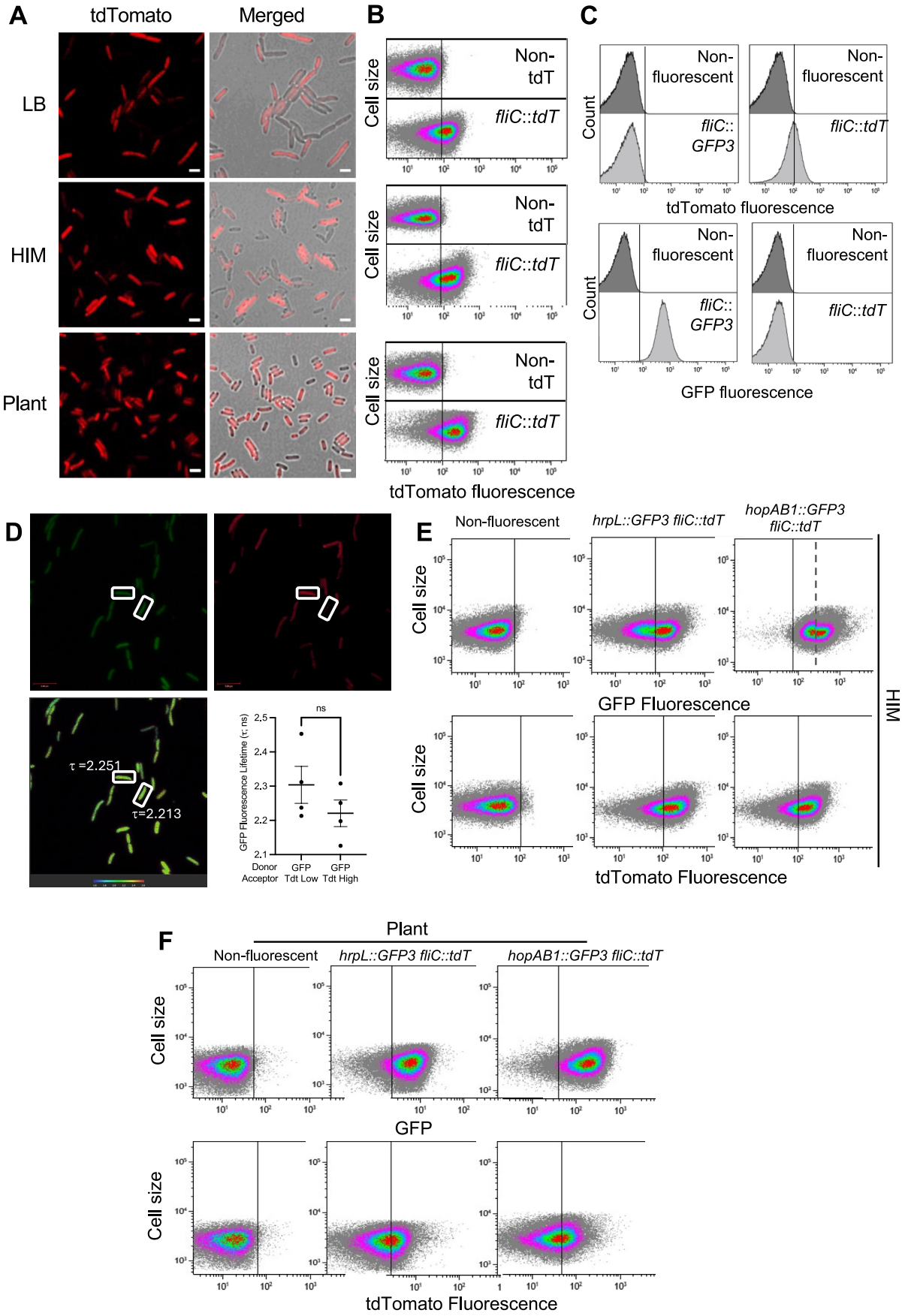

Extended Data Fig. 3 | See next page for caption.

https://doi.org/10.1038/s41564-025-01966-0

Extended Data Fig. 3 | Flagella display heterogenous expression in *Pseudomonas syringae*. (**a**) CSLM of a strain carrying *fliC*::*tdT* grown O/N in LB (upper), or 24 h in HIM (central), or extracted from bean leaf apoplasts 4 dpi (bottom). tdTomato panels show tdTomato fluorescence as reporter of *fliC* expression and BF panel corresponds to bright field. Scale bars correspond to 2 µm. Images are representative of 3 independent experiments (**b**) FC analysis of *fliC*::*tdT* strain in conditions described in **a**. Dot plots show cell size *versus* tdTomato fluorescence intensity, represented as arbitrary units in logarithmic scale. Data collected for 100,000 events per sample. The non-tdT graph show autofluorescence levels displayed by wild type not carrying any fluorescent gene. Vertical lines leave 99% of data of non-tdT strain to the left and is used as reference to differentiate for OFF cells. **a** and **b** show representative results of at least three independent replicates. (**c**) FC analysis shows *GFP3* and *TdTomato* fluorescence detection is not bias by bleed through. Left graphs correspond to *fliC*::*GFP3* strain and right to the *fliC*::*tdT* strain. Upper graphs show tdTomato fluorescence *versus* cell count and bottom graphs show GFP fluorescence *versus* cell count. In all cases the non-fluorescent strain is included as negative control and data were treated as in **b**. (**d**) Quantification of GFP lifetime (τ) in the presence or absence of tdTomato. Bacteria expressing similar levels of *hrpL*::*GFP3* (determined as GFP fluorescence intensity) and differing in the expressing of *fliC*::*tdT* expression (as shown by different tdTomato fluorescence intensity) were chosen for the analysis (upper panel). GFP lifetime was obtained for each pixel of the image (lower-left) and mean was calculated for each single bacterium. Average of four bacteria in each condition is represented (lower-right) and statistical significance determined with a t-test. (**e** and **f**) Dot plot graphs display fluorescence intensity of GFP or tdTomato *versus* cell size in non-fluorescent bacteria (wild type), or strains carrying *hrpL*::*GFP3 fliC*::*tdT* or *hopAB1*::*GFP3 fliC*::*tdT* corresponding to data shown in Fig. 4 as GFP fluorescence *versus* that of tdTomato. Figure show representative results of at least three independent experiments. In (**e**), bacteria grown 24 h in HIM after diluting an O/N LB culture, display reproducible bistable expression of both *hrpL*::*GFP3* and *hopAB1*::*GFP3* and heterogeneous (occasionally bistable) expression of *fliC*::*tdT*. In the case of *hopAB1*::*GFP3 fliC*::*tdT* strain in HIM, an additional vertical line (dashed) was added to separate the subpopulations differing in *hopAB1* expression, which is higher due to the high basal levels of this gene. In (**f**), bacteria extracted from bean leaf apoplasts 4 dpi display typical heterogeneous (never bistable) expression of *hrpL*::*GFP3, hopAB1*::*GFP3* and *fliC*::*tdT*.

https://doi.org/10.1038/s41564-025-01966-0

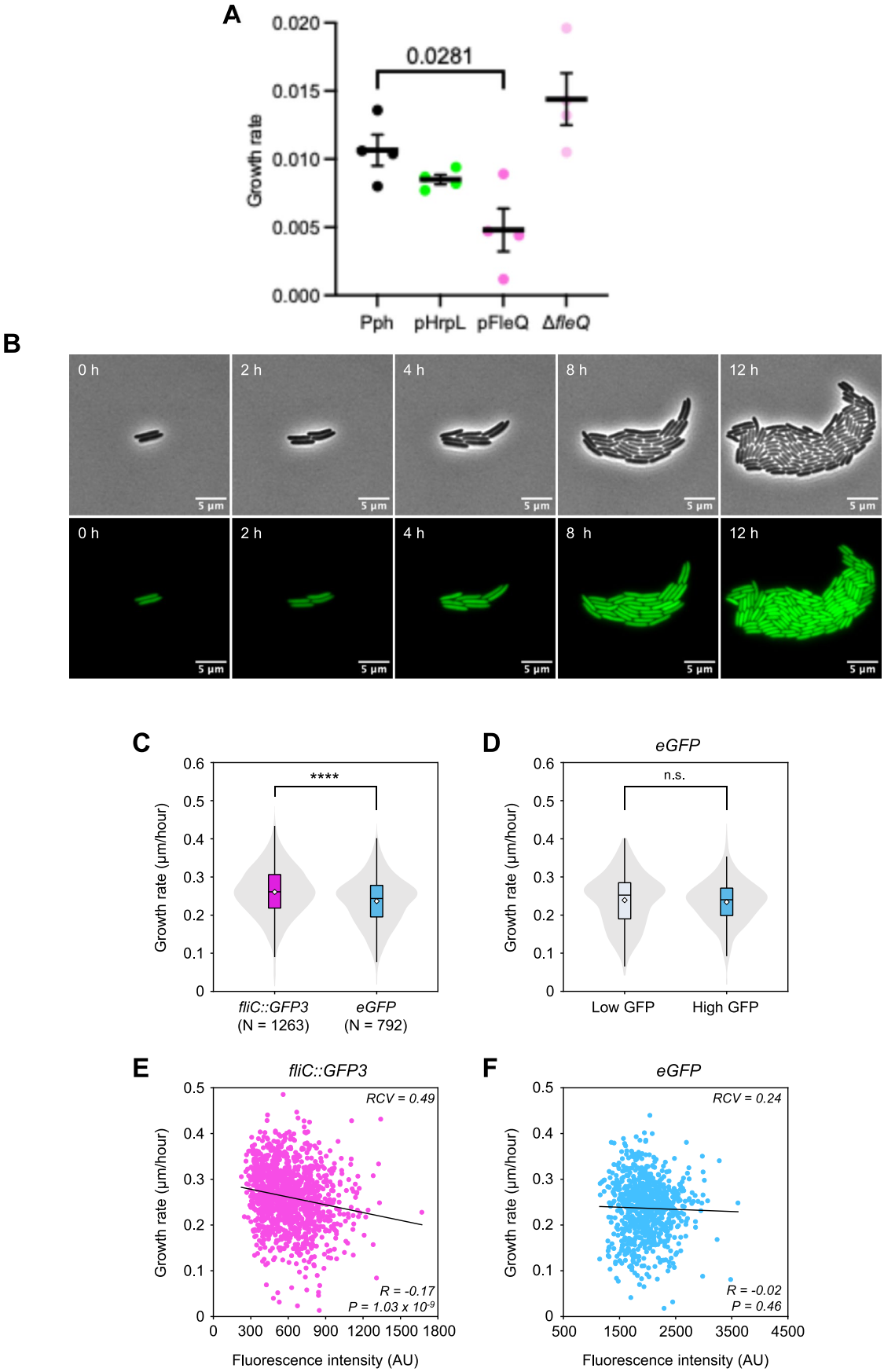

Extended Data Fig. 4 | See next page for caption.

https://doi.org/10.1038/s41564-025-01966-0

Extended Data Fig. 4 | T3SS and flagella expression impact on bacterial growth and growth cost associated with single cell levels of flagella production is not due to GFP. (**a**) Growth rates of 1448 A wild type, a derivative carrying a plasmid that determines constitutive expression of *hrpL* (pHrpL), or of *fleQ* (pFleQ), or a *fleQ* deletion *(ΔfleQ)*, in HIM. Data correspond to 4 biological replicates. Data are presented as mean values +/− SEM. Significative differences are observed between WT and pFleQ strains according to a one-way ANOVA followed by Tukey's multiple comparison test ($P < 0.05$). P value is indicated in the graph. (**b**) Selected timelapse images of wild type constitutively expressing GFP (eGFP) during the microcolony development on agar pads in phase contrast (top) and GFP fluorescence (bottom) channels. Contrast and brightness were adjusted and maintained throughout. (**c**) Comparisons of mean growth rates for *eGFP* strain and *fliC*::*GFP3* strain. Note that GFP in the *eGFP* strain has a much higher fluorescence intensity compared to *fliC*::*GFP3*. *eGFP* shows a significantly lower average growth rate compared to *fliC*::*GFP* (Mann-Whitney U test, $P = 7.7 \times 10^{-15}$). (**d**) Comparison of growth rate of cells displaying high or low GFP signal (determined by splitting the population into two groups using the median fluorescence intensity value) for eGFP strain shows no significant differences between growth rates of cells expressing high or low GFP levels (Mann-Whitney U test, $P < 0.05$). (**e**) Correlation between growth rates and fluorescence intensity of individual *fliC::GFP3* cells indicates that higher *fliC* expression is associated with slower growth. The shaded area shows the 95% confidence interval. (**f**) Correlation between growth rates and fluorescence intensity of individual eGFP cells indicates that higher GFP expression is not associated with slower growth. The shaded area shows the 95% confidence interval.

https://doi.org/10.1038/s41564-025-01966-0

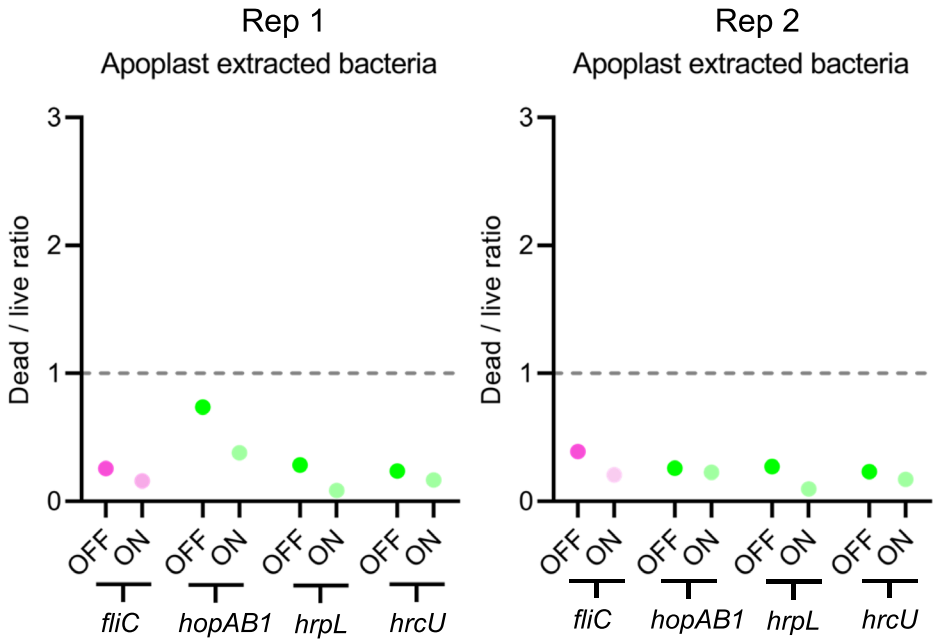

Extended Data Fig. 5 | Dead-live staining shows neither bias towards Flagella^{ON} cells nor for T3SS^{OFF} cells during plant growth. Graph shows the dead/live ratio for bacteria either expressing or not *fliC*::*GFP3*, *hrpL*::*GFP3*, *hopAB1*:*GFP3* or *hrcU*::*GFP3* during plant growth. Apoplast-extracted bacteria at 4 dpi in bean leaves were stained with a solution of Propidium iodide (PI). Data were obtained by flow cytometry analysis (100,000 events/ per replicate) and GFP levels were used to differentiate between ON and OFF cells using the non-fluorescent wild type strain as reference, as indicated before. Fluorescence of PI was used to differentiate dead and alive bacteria comparing to the non-fluorescent wild type. Each dot represents biological replicate in two different experiments (Rep 1 and Rep 2).

https://doi.org/10.1038/s41564-025-01966-0

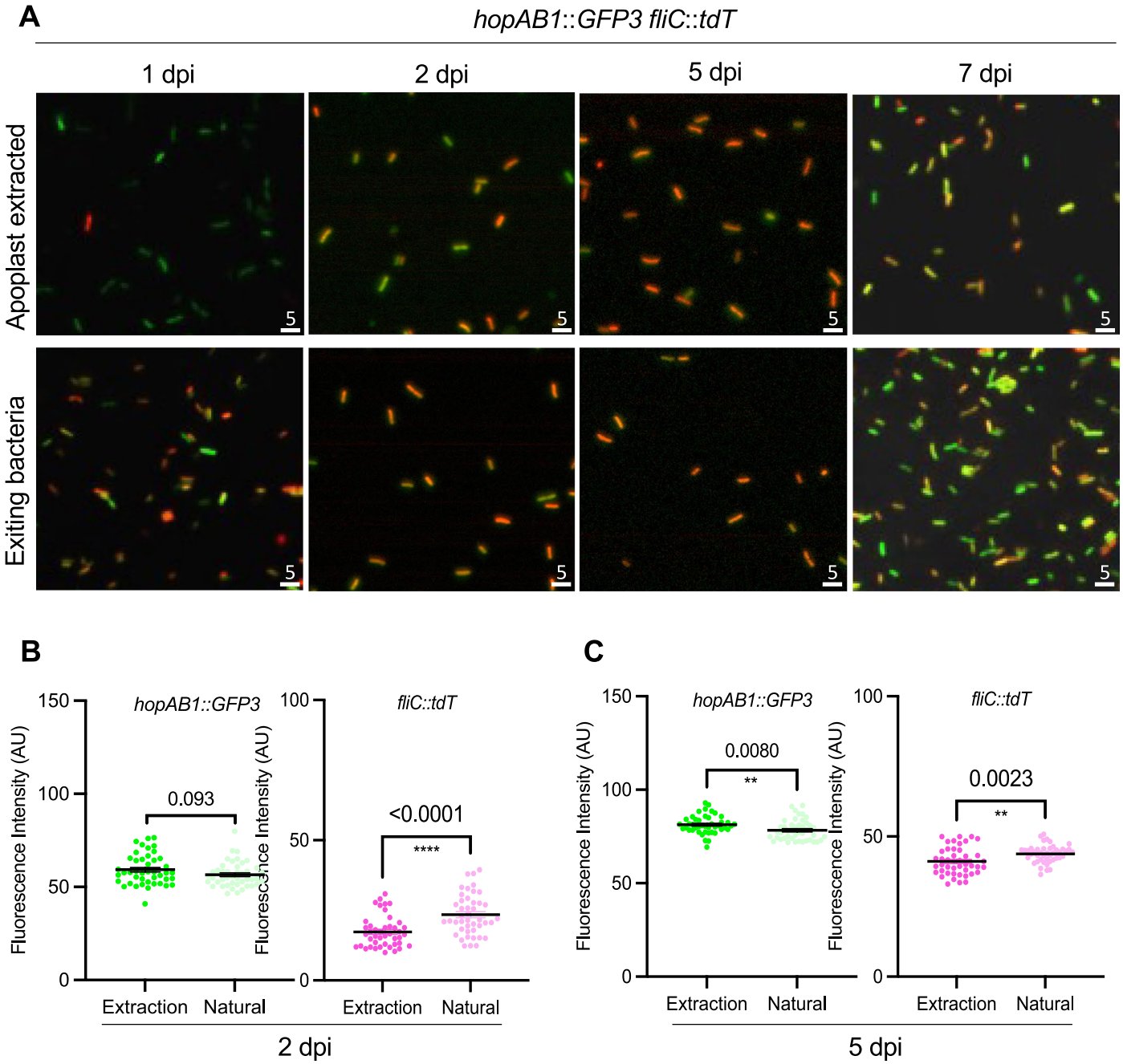

Extended Data Fig. 6 | Active exit from infected tissues is preferentially carried out by Flagella^{ON} bacteria. (**a**) Selected images of apoplast-extracted bacteria (using negative pressure; upper panels) or bacteria exiting the tissue on their own (during leaf incubation within a $MgCl_2$ solution; natural exit, lower panels) at 1 dpi and 2 dpi (asymptomatic tissue), or 5 dpi (just before visible symptoms appear) and 7 dpi (fully symptomatic necrotic tissue). Contrast and brightness were adjusted to improve visualization but were kept constant across the different conditions. (**b** and **c**) Fluorescence quantification of the images obtained in **a** for 2 dpi and 5 dpi using Fiji software. Graph shows arbitrary units of GFP fluorescence, corresponding to the expression of the T3SS gene fusion *hopAB1::GFP3* in the samples, or tdTomato fluorescence corresponding to the expression of *fliC::tdT*. Each dot corresponds to an individual bacterium (n = 44) as analyzed from the image. Comparisons between apoplast extraction and natural exit were carried out per each sample using an unpaired two-tailed t-test. Data are presented as mean values +/− SEM. Graphs show results representative of 3 independent experiments.

https://doi.org/10.1038/s41564-025-01966-0

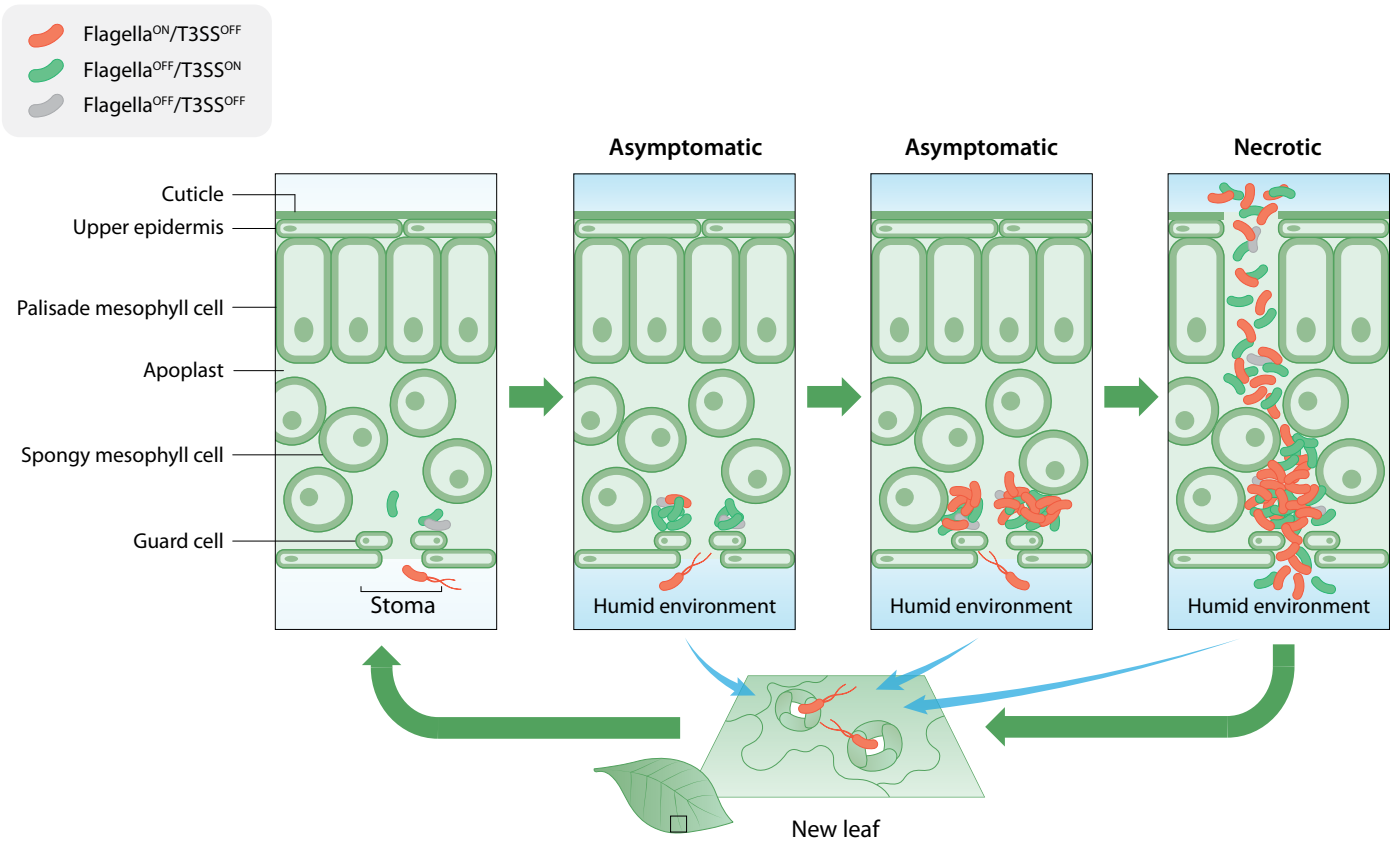

Extended Data Fig. 7 | T3SS and flagella phenotypic heterogeneity overlays with dynamic and spatial expression patterns during interaction with the plant host. Model summarizes the dynamic of expression of these two loci during in planta growth. Starts at the beginning of the infection (top left). A leaf section with different structural elements indicated, illustrates entry of swimming bacteria into the apoplast through a stoma, where bacteria expression profiles switch from Flagella^{ON}/T3SS^{OFF} to start the interaction with host-cell needed to suppress defences and to allow bacterial multiplication. During the initial multiplication (1 dpi) bacteria maintain a predominant Flagella^{OFF}/T3SS^{ON} expression profile with orthogonal stochastic switching to T3SS^{ON}, regardless of flagellar expression which is reduced to a very limited proportion of the population. However, Flagella^{ON} bacteria are particularly capable of exiting the leaf within a humid environment and the exiting population is enriched in Flagella^{ON} bacteria. As the microcolony grows those bacteria closest to the host cell remain T3SS^{ON} with the occasional stochastic switch to T3SS^{OFF}, but the growing side of the microcolony, father away from the host cell switch to Flagella^{ON}/T3SS^{OFF}. The latter also show overlaid stochastic heterogeneity. When the infection reaches the last stages and the plant tissue becomes necrotic, bacteria of all phenotypic combinations exit the compromised tissue in wet environments. Bacteria exiting the tissues at all the stages of the infection can potentially move onto a new niche or host. Red bacteria indicate Flagella^{ON}/T3SS^{OFF} bacteria, and green bacteria Flagella^{OFF}/T3SS^{ON}, although bacteria expressing both to different levels can also be found. Grey bacteria indicate stochastically OFF bacteria for either locus.

nature portfolio

Corresponding author(s): Carmen R. Beuzón

Last updated by author(s): Feb 14, 2025

Reporting Summary

Nature Portfolio wishes to improve the reproducibility of the work that we publish. This form provides structure for consistency and transparency in reporting. For further information on Nature Portfolio policies, see our Editorial Policies and the Editorial Policy Checklist.

Statistics

For all statistical analyses, confirm that the following items are present in the figure legend, table legend, main text, or Methods section.

n/a	Confirmed	
☐	☒	The exact sample size (*n*) for each experimental group/condition, given as a discrete number and unit of measurement
☐	☒	A statement on whether measurements were taken from distinct samples or whether the same sample was measured repeatedly
☐	☒	The statistical test(s) used AND whether they are one- or two-sided *Only common tests should be described solely by name; describe more complex techniques in the Methods section.*
☒	☐	A description of all covariates tested
☒	☐	A description of any assumptions or corrections, such as tests of normality and adjustment for multiple comparisons
☐	☒	A full description of the statistical parameters including central tendency (e.g. means) or other basic estimates (e.g. regression coefficient) AND variation (e.g. standard deviation) or associated estimates of uncertainty (e.g. confidence intervals)
☐	☒	For null hypothesis testing, the test statistic (e.g. *F*, *t*, *r*) with confidence intervals, effect sizes, degrees of freedom and *P* value noted *Give P values as exact values whenever suitable.*
☒	☐	For Bayesian analysis, information on the choice of priors and Markov chain Monte Carlo settings
☒	☐	For hierarchical and complex designs, identification of the appropriate level for tests and full reporting of outcomes
☐	☒	Estimates of effect sizes (e.g. Cohen's *d*, Pearson's *r*), indicating how they were calculated

Our web collection on statistics for biologists contains articles on many of the points above.

Software and code

Policy information about availability of computer code

Data collection	LAS X (Leica microsystem; https://www.leica-microsystems.com/es/productos/software-de-microscopia/p/leica-las-x-ls/); ZEN 3.4 (Carl Zeiss Microscopy; https://www.zeiss.com/m icroscopy /es/productos/software/zeiss-zen .html); BDFACSDiva 9.0.1 (BD; https:// www .bdbiosciences.com/ ko-kr/products/software/instrument-software/bd-facsdiva-software); BD FACSuite 1.0.5 (BD; https://www.bdbiosciences.com/en-ie/ products/software/instrument-software/bd-facsuite-application#Overview)
Data analysis	Image J/Fiji 2.14.0 (https://imagej.net/ij/docs/index.html); GraphPad Prism 9 (Prism; https://www.graphpad.com); Kaluza Analysis (Beckman Coulter; https://www.beckman.es/flow-cytometry/software/kaluza); FlowJo Xv. 10.0.7 (Tree Star; https://www.flowjo.com) ;DeLTA 2.0 (O'Connor,0 . M.,A Inahhas,R . N.,L ugagne,J . -B.,& Dunlop,M . J. DeLTA 2.0: A deep learning pipeline for quantifying single-cell spatial and temporal dynamics. PLoS Comput Biol 18,e 1009797. 10.1371/journal.pcbi.1009797 (2022); https://github.com/Jluneau/ Pseudomonas_AgarPads_fliC)

For manuscripts utilizing custom algorithms or software that are central to the research but not yet described in published literature, software must be made available to editors and reviewers. We strongly encourage code deposition in a community repository (e.g. GitHub). See the Nature Portfolio guidelines for submitting code & software for further information.

Data

Policy information about availability of data

All manuscripts must include a data availability statement. This statement should provide the following information, where applicable:

- Accession codes, unique identifiers, or web links for publicly available datasets
- A description of any restrictions on data availability
- For clinical datasets or third party data, please ensure that the statement adheres to our policy

Raw data for all figures and extended figures have been published at Zenodo and the corresponding DOIs listed in the reference section of the manuscript file. All except imaging data from time-lapse studies that are available at https://www.ebi.ac.uk/biostudies/bioimages/studies/S-BIAD1413.

Research involving human participants, their data, or biological material

Policy information about studies with human participants or human data. See also policy information about sex, gender (identity/presentation), and sexual orientation and race, ethnicity and racism.

Reporting on sex and gender	Not applicable
Reporting on race, ethnicity, or other socially relevant groupings	Not applicable
Population characteristics	Not applicable
Recruitment	Not applicable
Ethics oversight	Not applicable

Note that full information on the approval of the study protocol must also be provided in the manuscript.

Field-specific reporting

Please select the one below that is the best fit for your research. If you are not sure, read the appropriate sections before making your selection.

☒ Life sciences ☐ Behavioural & social sciences ☐ Ecological, evolutionary & environmental sciences

For a reference copy of the document with all sections, see nature.com/documents/nr-reporting-summary-flat.pdf

Life sciences study design

All studies must disclose on these points even when the disclosure is negative.

Sample size	No statistical method was used to predetermine sample size. Sample sizes were chosen on the bases of the sample sizes commonly used for the type of assay as specified on the indicated references (doi: 10.1111/j.1364-3703.2008.00511; doi: 10.1111/j.1364-3703.2007.00404.x; doi: 10.1093/nar/gkaa730; doi: 10.1038/s41598-018-33137-z) and common in similar studies (doi: 10.1371/journal.pone.0035871; doi: 10.4161/psb.5.12.1384; doi: 10.1094/MPMI-23-9-1197; doi: 10.1007/978-1-4939-3115-6_17; doi: 10.1016/s1286-4579(01)01496-4; doi: 10.1093/emboj/19.13.3235; doi: 10.1073/pnas.2322371121; doi: 10.1038/s41467-024-47114-w; doi: 10.3389/fcimb.2023.1146070; doi: 10.1073/pnas.2203011119; doi: 10.1093/nar/gkz530; doi: 10.1371/journal.pgen.1007677; doi: 10.1371/journal.pgen.100566; doi: 10.1038/srep42068). Experiments include between 3-5 biological replicates and were independently replicated between 2-5 times depending on the inter-and intra-replicate variability observed. Details of the analysis used, and specific P-values are indicated in the figure legends of each experiment, in all or at least significantly different values. Reproducibility was tested in independent experiments and the total number of biological replicates indicated in each figure legend.
Data exclusions	No data were excluded from the analyses, except for Fig. 1A, Fig. 5B and Extended Data Fig. 6B and 6C in which, to adjust the sample size (n value) between conditions, some data were excluded following blind elections.
Replication	Independent experiments and biological replicates were carried out to verify the reproducibility of the experimental findings. All attempts at replication were successful and the variation observed is reflected on the results shown in the manuscript. The exact number of independent experiments and biological replicates is indicated for each figure either within the actual figure or its legend. Details on statistics are also included in the legends and expanded on the corresponding methods section.
Randomization	No randomization was performed. Bacterial cultures and assays were always carried out under homogenous controlled environments and were always genetically homogenous (clonal cultures) from a reference strain or strain derivates generated by our laboratory and fully defined in this or previous reports (as referenced). Assays including plants use a single commercially verified plant variety and are always carried out in homogeneous controlled enrivonments.
Blinding	Data collection and analysis was not carried out blindly. Assays employed involved automated data collection (except straightforward colony

Blinding

counts) and analysis was software-supported whenever possible. When not possible, such as when describing non-quantifiable microscopy data was collected, the fact that only one sample type was analyzed therefore made blinding not possible.

Reporting for specific materials, systems and methods

We require information from authors about some types of materials, experimental systems and methods used in many studies. Here, indicate whether each material, system or method listed is relevant to your study. If you are not sure if a list item applies to your research, read the appropriate section before selecting a response.

Materials & experimental systems

n/a	Involved in the study
☒	☐ Antibodies
☒	☐ Eukaryotic cell lines
☒	☐ Palaeontology and archaeology
☒	☐ Animals and other organisms
☒	☐ Clinical data
☒	☐ Dual use research of concern
☐	☒ Plants

Methods

n/a	Involved in the study
☒	☐ ChIP-seq
☐	☒ Flow cytometry
☒	☐ MRI-based neuroimaging

Dual use research of concern

Policy information about dual use research of concern

Hazards

Could the accidental, deliberate or reckless misuse of agents or technologies generated in the work, or the application of information presented in the manuscript, pose a threat to:

No	Yes	
☒	☐	Public health
☒	☐	National security
☒	☐	Crops and/or livestock
☒	☐	Ecosystems
☒	☐	Any other significant area

Experiments of concern

Does the work involve any of these experiments of concern:

No	Yes	
☒	☐	Demonstrate how to render a vaccine ineffective
☒	☐	Confer resistance to therapeutically useful antibiotics or antiviral agents
☒	☐	Enhance the virulence of a pathogen or render a nonpathogen virulent
☒	☐	Increase transmissibility of a pathogen
☒	☐	Alter the host range of a pathogen
☒	☐	Enable evasion of diagnostic/detection modalities
☒	☐	Enable the weaponization of a biological agent or toxin
☒	☐	Any other potentially harmful combination of experiments and agents

Plants

Seed stocks	Phaseolus vulgaris var. Canadian Wonder (https://www.sativa.bi0/en/canadian-wonder-bol6)
Novel plant genotypes	No novel plant genotypes were generated
Authentication	Not applicable

Flow Cytometry

Plots

Confirm that:

☒ The axis labels state the marker and fluorochrome used (e.g. CD4-FITC).

☒ The axis scales are clearly visible. Include numbers along axes only for bottom left plot of group (a 'group' is an analysis of identical markers).

☒ All plots are contour plots with outliers or pseudocolor plots.

☒ A numerical value for number of cells or percentage (with statistics) is provided.

Methodology

Sample preparation	Cytometry samples were obtained from bacterial cultures or from infected plant tissue as detailed in the methodology section
Instrument	BD FACS Verse cytometer (BD Biosciences, USA) for analysis BD FACSAriaTM Fusion flow cytometer (BD Biosciences, USA) for cell sorting. MoFloTM XDP cytometer (Beckman Coulter, USA) for cell sorting.
Software	To acquire Flow cytometry data for analysis BDFACSuite software was used. To generate graphs Kaluza software was used. To acquire flow cytometry data for cell sorting BDFACSDiva was used. To analyze flow cytometry data from cell sorting FlowJo and Kaluza was used Kaluza Analysis 2.1 (Beckman Coulter; https://www.beckman.es/flow-cytometry/software/kaluza) B D F ACS Diva 9.0.1 (B D; https ://www. bd biosciences. co m/ko-kr / prod u cts/softwa re/instrument -softwa re/bd-fa csdiva-softwa re) BD FACSuite 1.0.5 (BD; https://www .bdbiosciences.com/en-ie/products/software/i nstru ment-software/ bd-facsuite-application#Overview) FlowJo Xv. 10.0.7r (Tree Star; https://www.flowjo.com)
Cell population abundance	Cell population abundancy was determined as 100,000 events included in the performed gates
Gating strategy	To acquire data, circular gates expanding out from the FSC and SSC mean were performed to include events enriched in particle with bacterial size. After acquisition, all SSC, FSC, and fluorescence zero values were excluded to generate graphs

☒ Tick this box to confirm that a figure exemplifying the gating strategy is provided in the Supplementary Information.